# DEVELOPMENT OF MULTI-AXIS LASER MICROMACHINING SYSTEM SUITABLE FOR MACHINING NON-LINEAR CONTOURED SURFACES

A THESIS SUBMITTED TO

THE GRADUATE SCHOOL OF ENGINEERING AND SCIENCE

OF BILKENT UNIVERSITY

IN PARTIAL FULFILLMENT OF THE REQUIREMENTS FOR

THE DEGREE OF

MASTER OF SCIENCE

IN

MECHANICAL ENGINEERING

By

Serhat Kerimoğlu

August 2016

DEVELOPMENT OF MULTI-AXIS LASER MICROMACHINING SYSTEM SUITABLE FOR MACHINING NON-LINEAR CONTOURED SURFACES
By Serhat Kerimoğlu
August 2016

We certify that we have read this thesis and that in our opinion it is fully adequate, in scope and in quality, as a thesis for the degree of Master of Science.

Melih Çakmakcı(Advisor)

Yiğit Karpat

Uluç Saranlı

Approved for the Graduate School of Engineering and Science:

Levent Onural
Director of the Graduate School

# ABSTRACT

## DEVELOPMENT OF MULTI-AXIS LASER MICROMACHINING SYSTEM SUITABLE FOR MACHINING NON-LINEAR CONTOURED SURFACES


Serhat Kerimoğlu
M.Sc. in Mechanical Engineering
Advisor: Melih Çakmakcı
August 2016


In recent years, studies on manufacturing systems have proved the importance of cooperation of positioning systems with laser cutting technology. The performance of the manufacturing system can be improved by utilizing both laser and positioning systems together.

In this study, design and development of a micromachining system which can perform on non-linear contoured surfaces is presented. Laser micromachining system is designed and assembled including a nanosecond Q-switched pulsed fiber laser, a 6-DOF hexapod manipulator, a granite table in order to absorb vibrations and an external cabin system to isolate the whole system for safety and health issues. Performance characteristics of micromachining devices mainly determined by precision and characteristics of each individual components of the system. Therefore, the studies to improve the performance of the laser micromachining system are related with laser, isolation and positioning systems.

A dynamic model of the positioning system is derived to obtain the control parameters for the actual positioning system. By using these parameters, the performance of the laser micromachining system on nonlinear contoured surface is improved and discussed in detail. The simulation environment MATLAB/SimMechanics is used to model the dynamics of the positioning system. With the kinematic and dynamic model of the manipulation system simulations, significant performance enhancements are obtained on non-linear contoured surfaces.


*Keywords:* Manufacturing, Parallel Manipulators, Laser Micromachining, Kinematics, Performance Improvements.

# ÖZET

# DOĞRUSAL OLMAYAN YÜZEYLERDE ÜRETİM YAPABİLECEK LAZER MİKRO İŞLEME SİSTEMİ GELİŞTİRİLMESİ

Serhat Kerimoğlu
Makina Mühendisliği, Yüksek Lisans
Tez Danışmanı: Assistant Professor Melih Çakmakcı
Ağustos 2016

Son yıllarda, üretim sistemleri üzerine yapılan çalışmalar lazer mikro işleme teknolojisi ile pozisyonlama sistemlerinin işbirliğinin önemini ortaya koymuştur. Üretim sisteminin performansı hem lazer hemde pozisyonlama sistemlerinin performanslarını göz önüne alarak geliştirilebilir.

Bu çalışmada, doğrusal olmayan yüzeylerde mikro işleme yapabilecek bir lazer mikro üretim sistemi tasarlanmış ve geliştirilmiştir. Geliştirilen lazer mikro işleme sistemi bir adet nanosecond Q-switched pulsed fiber laser, 6 serbestlik dereceli hexapod manipülatör, titreşimleri emmek için kullanılan granitten üretilmiş bir masa ve güvenlik ve sağlık önlemleride düşünülerek üretim sistemini çevresel etkenlerden koruyacak bir dış kabinden oluşmaktadır. Mikro üretim sistemlerinin performans özellikleri, her bir bileşeninin kendine özgü hassasiyeti ve diğer özellikleri ile belirlenir. Bundan dolayı, geliştirilen lazer mikro işleme sisteminin performansını geliştirme çalışmaları lazer sistemi, izolasyon sistemi ve pozisyonlama sistemi üzerinden tamamlanmıştır.

Pozisyon kontrol çalışmaları yapabilmek için, kullanılan pozisyonlama sisteminin bir dinamik modeli çıkarılmıştır. Elde edilen dinamik modeli kullanarak kontrol parametreleri bulunmuş, ayrıntılı olarak ele alınmış ve sistemin performansı artırılmıştır. Pozisyonlama sisteminin dinamik modeli çıkarılırken MATLAB / SimMechanics simülasyon programı kullanılmıştır. Modellenen kinematik özellikler ve dinamik model kullanılarak yapılan testler ve simülasyonlar doğrulturunda, doğrusal olmayan yüzeylerde önemli performans geliştirmeleri gerçekleştirilmiştir.

*Anahtar sözcükler*: Üretim, Parallel Manipulatörler, Lazer Mikro Üretim, Kinematik.

# Acknowledgement

I would like to express the deepest appreciation to my advisor, Assist. Prof. Melih Çakmakcı for his constant guidance and support during the studies contained in this work. His directives and encouragements are the most crucial part of the completion of this thesis.

I am thankful to Mechanical Engineering Department of İ.D. Bilkent University with all of its staff for their precious contibutions.

I would also like to appreciate Assoc. Prof. Dr. Yiğit Karpat and Dr. Şakir Baytaroğlu for their valuable advices and technical guidance with very trusting assistance.

My parents are the most supreme part of this study by their invaluable support with their love and my brother Deniz Kerimoğlu stands on an unforgetable place on my research.

Finally, I would like to thank to my dear friends Barış Taner, Buğra Türeyen, Mümtazcan Karagöz and Alper Tiftikçi for their friendship with wonderful and powerful support.

# Contents

# List of Figures

# List of Tables

# Chapter 1

# Introduction

Over the recent years, there is a rising interest on laser micromachining systems for many research and industrial applications. Laser micromachining technology has drawn attention among other micromanufacturing technologies by its incomparable advantages. Laser technology integrates a non contact and forceless machining technique with micromanufacturing technology. With this integration, laser micromachining systems offer many advantages when compared to conventional manufacturing systems. Some of these advantages can be listed as material variation, absence of machining tools, process time and diversity of laser systems that eliminates scale considerations of manufacturing. Laser micromachining systems are capable of achieving one micron featuring with submicron precision and it ables to perform on almost any material. Laser micromachining systems are being used in many industrial areas and it is a cost effective system for both small and large volume applications. Some of these applications are biomedical catheter hole drilling, micro-electro-mechanical system (MEMS) fabrication applications, ink jet printer nozzle, microfluidics and production of plastic microlens arrays [1], [2], [3], [4].

A laser micromachining system mainly consist of a laser machine which generates the laser beam, a beam delivery system that directs the laser beam to the workpiece and a positioning system to move the workpiece. Beam delivery part of the overall system also includes a beam deflection property. Deflection and positioning systems can operate very fast and precisely in a limited workspace. In order to get rid of workspace limitations and add some more dimensions, external positioning systems are need to be implemented to the overall system[5]. External positioning systems are used in laser micromachining systems to increase the overall system capabilities. Most of externally implemented positioning systems has translational degrees of freedoms on X, Y and Z axes [6]. There are some other laser micromachining systems which can operate on rotary axes [7]. According to the degrees of freedom properties of externally implemented positioning systems, laser micromachining process can be performed on nonlinear surfaces. To be able to perform on nonlinear surfaces, positioning system of laser micromachining system should have at least one rotational degree of freedom. Coronary stent manufacturing processes are the basic examples of such applications [8]. For more complex applications like manufacturing a 3D structure from a planar material, there is a laser type called Excimer laser. With an excimer laser, 3D materials can be manufactured in micrometer and nanometer scales [9]. There some other ways for 3D microstructures fabrication like lithograpgy and ultra precise diamond turning [10], [11].

In industry, there are some available commercial laser micromanufacturing systems which can perform on nonlinear surfaces [12]. They are mainly used for surface texturing and decoration. manufacturing method of these devices can be devided in to two cathegories. The first one can be considered as 2.5D machining and it is done by typically laser engraving. 3D surface is generated by the engraved volume from the surface according to the pattern on a planar surface. The second way is to perform directly on a 3D preprocessed surface[13]. In Figure 1.1, a 3D textured material is presented. Machining system which is used for these processes generally use serial robot arm for positioning the laser beam. Laser head is attached to the end effector of the positioning system. A laser machining system used for these processes is presented in Figure 1.2. Serial manipulators have large workspaces but they have problem in precise motions. As a result of this property of the serial manipulators, these laser texturing systems are not able to perform micromachining with high precision.

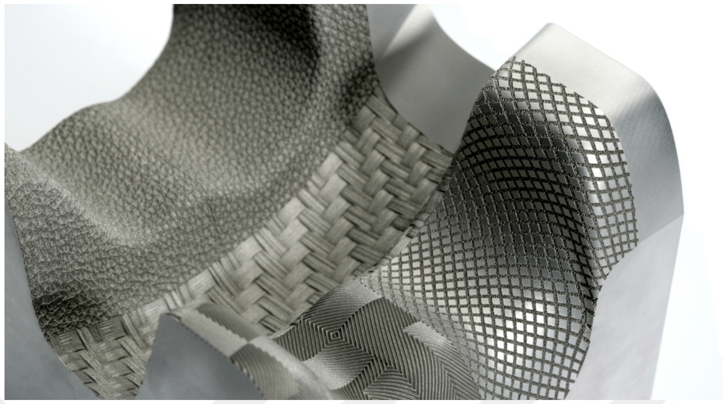

Figure 1.1: Laser Surface Texturing [14]

Figure 1.2: Robot Arm Laser Machine [15]

In literature, there is limited information about nonlinear surface texturing with laser micromachining systems. In [16], the authors give information about possible applications of laser microfabrication in 3D machining including dental threatment, cardiovascular implants and micro electronics.

A schematic representation of a laser micromachining system is presented in

Figure 1.3. As can be seen from the figure, laser micromachining system consists of a laser system, a positioning system and control systems with a computer. For many laser systems, beam collimator(narrows the laser beam), mirror (reflects the narrowed laser beam) and focus objective (optical lens, which focuses the laser beam on a point) are combined in a single system. Precision of positioning system and spot size of the laser system are the crucial components of the laser micromachining systems. Quality and characteristics of machined material depends on these components. Positioning system is another important component of a laser micromachining system. In a laser micromachining system, positioning system determines size, quality and shape of the workpiece. For high precision laser micromanufacturing systems, performance of the positioning system is one of the most important issue.

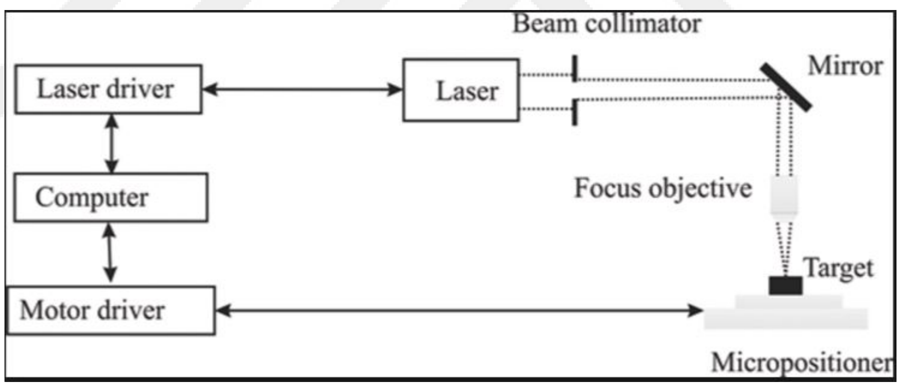


Figure 1.3: Schematic Representation of a Laser MicroMachining System [17]

In order to develop a laser micromachining system that can perform on nonlinear contoured surfaces, laser and positioning systems need to be combined perfectly. Properties of both systems are very important for a perfect combination. In addition to these components, some other systems must be added to the overall laser micromachining system. Because of the nature of the laser machining, unhealty material dust is released to the operation environmet. To prevent dangerous effects of this dust and isolate the overall system from the environment, external cabin systems are being used. Another necessary component for a high precision laser machining system is vibration absorber table. This absorber system is used for preventing the laser machining system from vibrational effects.

The main objective of this thesis is to develop a multi-axis laser micromachining system which is able to perform on nonlinear contoured surfaces. For this purpose, desired laser micromachining components are selected and integrated succusfully. A six degrees of freedom hybrid positioning system is used for positioning issues. The selected positioning system has fast and precise positioning capabilities with a wide range of work space. The laser system choosen for desired manufacturing system is a nanosecond pulsed fiber laser which can make machining in micrometer precision. For assembling the overall system and vibration isolation, a granite based table is designed. An external cabin is another component of the laser micromachining system. External cabin covers whole systems and provides isolation from the environment for safety and health considerations.

In this thesis, performance of laser system is optimized by implementing a new optical lens to the laser machine. The new lens decreased the measured spot size of the laser system and made it more precise for laser micromachining processes. Controller of the laser system is deactivated. By using a global laser projection protocole, laser beam generation machine is controlled by an external control device. This update provided us to change the power of the laser system during a machining process. After optimizing and updating laser system capabilities, positioning system is taken into account. Initially, a nonlinear trajectory is generated. The trajectory includes both translational and rotational motions and it requires the motion most of the actuators of the positioning system. With given trajectory, positioning system uses both serial and parallel manipulator properties of its hybrid structure while tracking it. The trajectory is for texturing on cylindrical surfaces and has some sharp corners which is considered as a challenge for positioning systems.

Kinematic analysis are performed for positioning system and dynamic model is generated in SimMechanics software for positioning system. Dynamic model is optimized by using measured manipulator system outputs. Various nonlinear trajectory tracking experiments and simulations are performed with the positioning system and dynamic model for various velocities. By utilizing these simulation and experimental results, PID controllers are designed for the dynamic model and finally, PID controller parameters of measured positioning system are tuned. PID controller parameter tuning studies are completed by using manual tuning technique. After the performance enhancements of the system are completed, a complex pattern is succesfully manufactured on a cylindrical surface of an aluminum material to demonstrate these enhancements.

This thesis is organized as follows; in Chapter 2, laser micromachining system components are described. Some improvements on laser machine and validation and calibration studies are presented by presenting several manufactured parts. Chapter 3 discusses kinematic analysis and SimMechanics model of positioning system. Improvement of control system of the positioning system by SimMechanics position control simulations and tuning manipulator default control parameters are presented in Chapter 4. Results of the validation and calibration studies for laser micromachining system are discussed in Chapter 5. Also, experimental and simulation results of contol system improvements are in the scope of Chapter 5. Chapter 6 contains conclusions of the performed studies and final comments.

# Chapter 2

# Machining System Setup

Laser micromachining systems are designed with some specific and necessary components in order to achieve specified processes. Selection of the components can be done with respect to the desired performance characteristics and the design assembly of the laser micromachining system can be considered according to the planned manufacturing process issues.

For afore laser micromachining system, the desired capability is in micrometer precision manufacturing on nonlinear contoured surfaces. System components are choosen for desired performance can be listed as,

- A laser beam generation machine with a micron level spot size

- A multi axis nano positioning system

- Cabin for isolation and health considerations

- A vibration absorber and stabilizer granite table

- Softwares and control systems.

Laser micromachining system components are choosen by taking assembly and integration considerations into account. They need to work together and operate in a feasible sized casing system.

In this chapter, a laser micromachining system, which is designed and integrated within the scope of this thesis is introduced. System components for the laser micromachining system is given and the overall systems validation, calibration and assembly studies are introduced. After completing assembly and integration studies and obtaining a working laser micromachining system, some improvements are made increase the performance of the laser micromanufacturing system. These additional studies are performed to improve system manufacturing capabilities intended to make micron precision laser machining on nonlinear contoured surfaces.

The first improvement is achieced by changing the power of the laser system during fabrication process. Performing fabrications with a smaller spot size than the original one is considered as an additional study to obtain various and desired surface characteristics in micron level precision. For this purpose, original control system of the laser machine is bypassed and a National Instruments Data Acquisition Card (NI DAQ) is integrated. To have a smaller spot size a new optical lens is implemented to the system. Validation experiments for the integrated NI DAQ and optical lens are done. Some of the experimental results for this studies are reported in this chapter. At the end of this chapter, some parts manufactured for validation of nonlinear surface texturing are presented. Established laser micromachining system is presented in Figure 2.1 and consist of four main parts. These are granite table for stability, external cabin for environmental isolation, laser and positioning system.

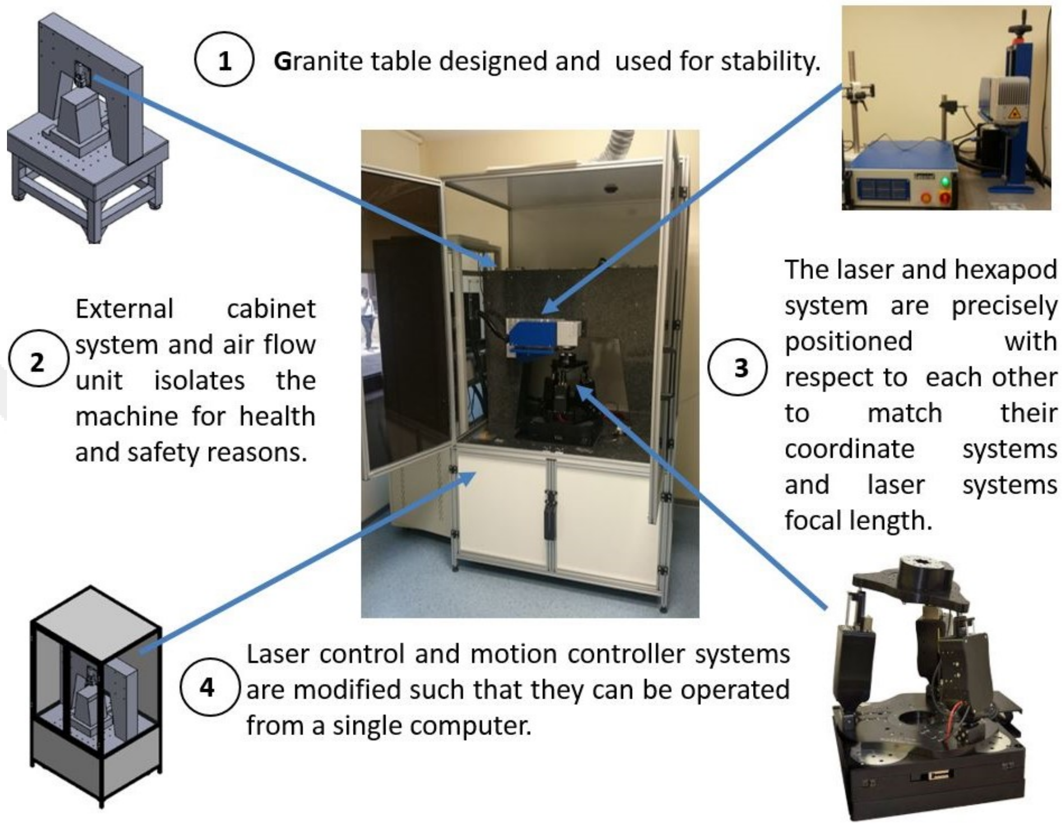


Figure 2.1: Laser Micromachining System Setup

## 2.1 Laser System

There are several laser systems for micromachining studies and selection of laser system is based on planned fabrications with these systems. Spot size is important for precision processing case and intensity is the main characteristics for cutting or surface texturing studies. After taking these issues and cost considerations into account, a Nanosecond Q-Switched Pulsed Fiber Laser is prefered to be used in laser micromachining system for micromachininig on nonlinear contoured surfaces.

The laser head that includes optical and beam positioning systems is mounted on the granite based table as can be seen on Figure 2.1. Laser system, which is used for micromachining processes is presented in Figure 2.2. Laser head including optical systems, control board (USB LMC Fiberlaser) and laser beam generation box (Max Photonics Q-Switch 10W Pulsed Fiber Laser) are also presented in Figure 2.2. The technical properties of this system can be seen in Figure 2.3.

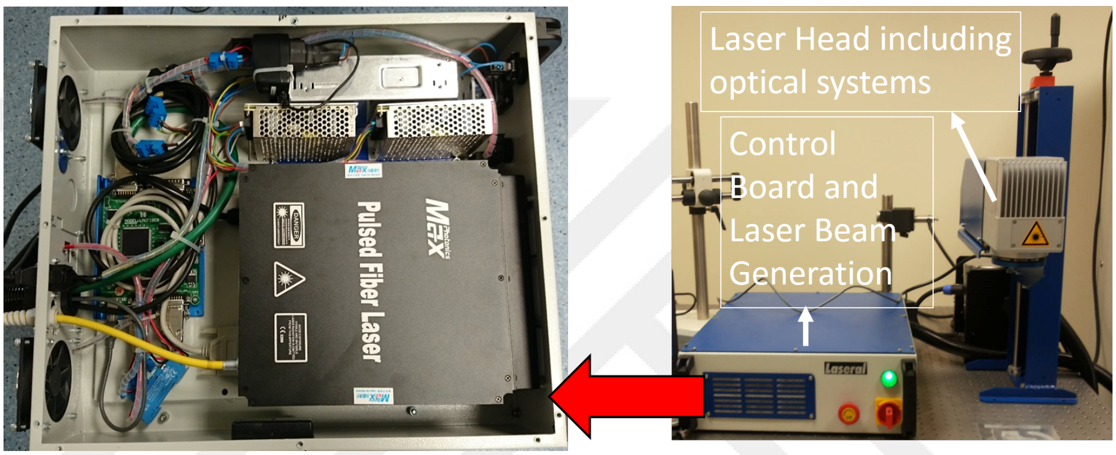


Figure 2.2: Laser Beam Generation System

As mentioned before, some specific properties of the laser system is modified by modifying and retuning some parts of the laser system. Original spot size of the laser system was about 70-80 microns. To have a better performance from the laser micromachining system, a smaller spot size is need to be obtained. In order to obtain smaller spot size, original 160 mm diameter optical lens of the system is replaced with a 56 mm diameter optical lens. Then, necessary calculations, experiments and optimizations studies are performed. With this modification, we obtained a spot size of about 10 micrometers. Also, this new lens has enabled some other improvements on laser system properties. These changes can be listed as the intensity of the laser beam and the focal length which is the optimum displacement between material and end point of the laser beam output of laser system.

| Parameter | Data | Unit |
|---|---|---|
| Type | MFP-10 | / |
| Central wavelength | 1064±4 | nm |
| Average output power | 10 | w |
| Energy per pulse | 0.5~0.6 | mJ |
| Pulse width | 80~120 | ns |
| Frequency tunable range | 22.7~79.4 | KHz |
| Polarization | Random | / |
| Beam quality | <1.4 | M2 |
| Beam diameter | 6~8 | mm |
| Power stability(t>5h) | <5 | % |
| Power tunable range | 5~100 | % |
| Fiber length | 1.9/2.5 | m |
| Operation volatage | 24 | VDC |
| Power consumption | 100 | W(20 Degree Celsius) |
| Clooing | Forced air | / |
| Operating temperature | 0~40 | Degree Celsius |
| Storage temperature | -10~60 | Degree Celsius |
| Isolator | standard | / |
| Dimension | W245x H111 x L317 | mm |

Figure 2.3: Laser System Properties [18]

## 2.2 Positioning System (Hexapod)

In laser micromachining systems, main and the most important component is the positioning system. The proper positioning system can be chosen with respect to the desired processes properties. Requirements can be devided into three different cathegories which are precision, work space and degrees of freedom of the positioning system. For our integration and design purposes, we use a nano precision hybrid hexapod system on ALIO INDUSTRIES. This positioning system provides 6 axis of freedom for material positioning with fast and precise manufacturing. The positioning system is a hybrid manipulator which consists of serial and a parallel chain and the system is composed of three parts. These parts are X-Y stage for translational motion on X and Y-axes, 3-RPS Tripod for translation in Z- axis and rotational motions on X and Y-axes (Roll(Theta X) and Pitch(Theta Y)). Remaining degree of freedom is added to the positioning system with a rotary motor that adds rotation about Z-axis (Yaw(Theta Z)).

Yaw motion which is performed by an additional rotary actuator is a redundant motion. Motions obtained by this actuator can be performed by other actuators of the positioning system. However, for this positioning system, yaw motion actuator increases workspace of the overall system and provides a fast and continuous manufacturing. It also enables to give comments to a single actuator for motion programs including yaw motion. Otherwise, trajectories which are including yaw motion need to be created with more complex motion programs and comments with remaining actuators of the positioning system.

Degree of freedom representation of the system can be seen in Figure 2.4. Also, technical properties on this positioning system are represented in the Figure 2.5.

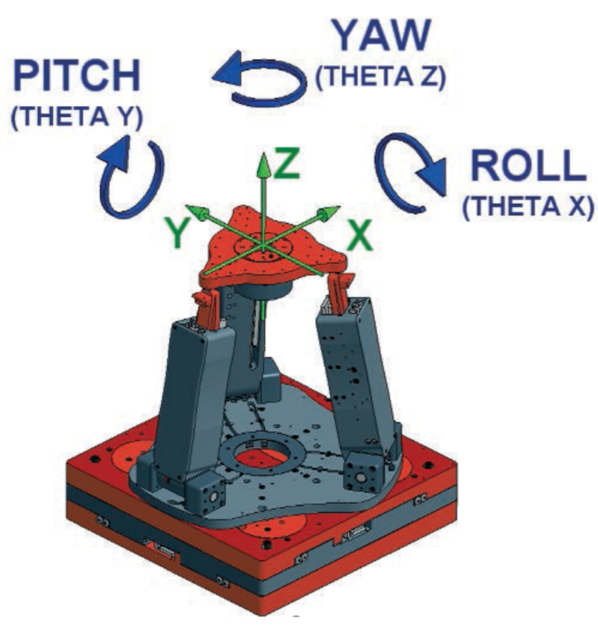


Figure 2.4: Hybrid Hexapod System and Degrees of Freedom [19]

| Specifications | Model: | AI-TRI-LM-5500 |
|---|---|---|
| Travel Range (Z) | | 55 mm |
| Travel Range (Pitch and Roll) | | ± 20° |
| **Performance Spec's (1): Precision Grade** | | (Std.) \| NANO |
| Linear Displacement Accuracy | | Contact ALIO Industries |
| Bi-Directional Linear Repeatability | | ± 100 nm |
| Angular Repeatability | | ~0.5 arc-sec |
| Linear Z-Axis Resolution | | 5 nm |
| Pitch and Roll Resolution | | ~0.02 arc-sec |
| Feedback | | Non-Contact Linear Encoder |
| Counterbalance Pressure (15) | | 54 psi |
| **Motion Profile Specifications** | | |
| Max Velocity (3) | | 0.2 m/sec |
| Max Angular Velocity (12) | | 90 deg/sec |
| Max Payload Capability (13) | | 10 kg |
| Max Center of Gravity Height (14) | | 75 mm |

Figure 2.5: Positioning System Properties [20]

### 2.2.1 Power PMAC

Positioning system uses Power PMAC Integrated Development Environment (IDE) family of motion and machine controller from Delta Tau Data Systems. Power PMAC system enables built in motion and device control applications with a multi purpose embedded computer. Programs and scripts can be developed by Power PMAC Script language or in C programming language and it provides script coding, debugging and testing developed programs.

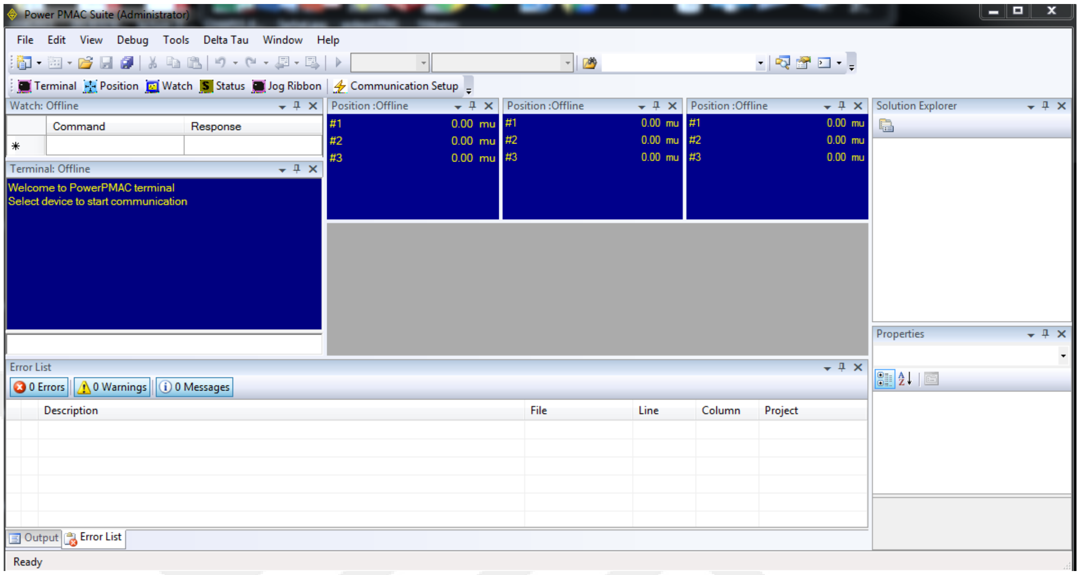


Figure 2.6: Power PMAC Interface

A screen shot of user interface of Power PMAC Suite is given in Figure 2.6. Power PMAC is an open source system that enables a powerful control for improvements on desired positioning strategies. Power PMAC system enables to follow measured and desired actuator positions and helps to perform better positioning.

The cabin has an air suction system to get rid of the unhealty dust and coloured glasses used in the cabin system to prevent unwanted light deflections.

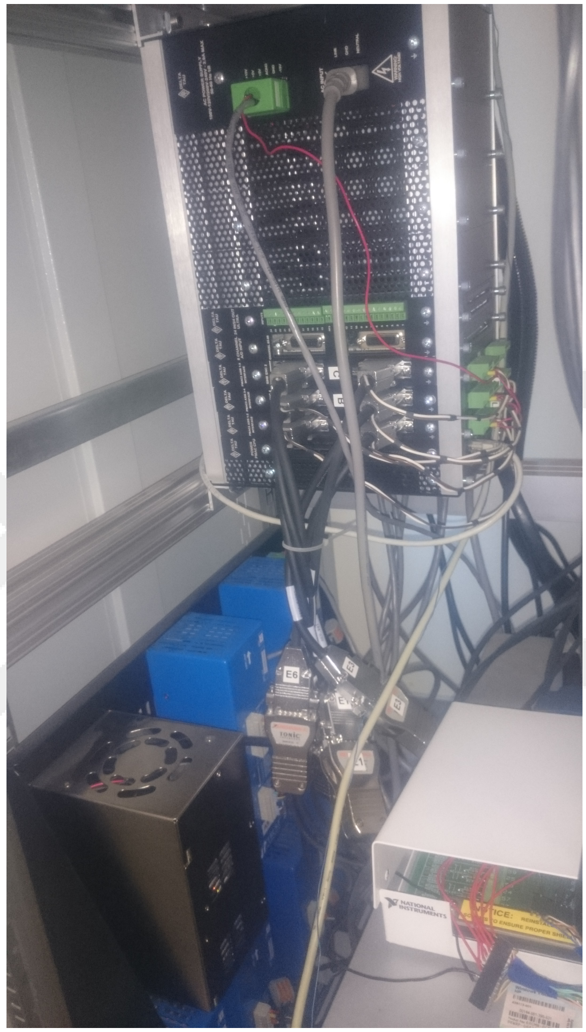

Figure 2.7: Hardware of Power PMAC

Figure 2.7 presents CPU, control board and amplifiers of the Power PMAC system. Power PMAC system has some extra control boards and they make some additional studies possible by importing external components.

## 2.3 Cabin and Stabilization System

In laser micromachining systems, vibrational and environmental isolation is another important issue. Due to the nature of laser machining process, various harmful material dust are being released to the air and the light generated by laser system during process causes some visual problems for the operator. In order to get rid of harmful effects of unhealty dust and light, laser micromachining system must be isolated from environment. These problems can be solved by developing an external cabin. Also, for micromachining process, isolation of the overall machining system from the ground is another important issue. Especially, the positioning system should be isolated from the ground to prevent external vibrational effects.

To obtain desired fabrications and results in a safety and healthy environment, a granite based vibration absorber table and a cabin with an air suction system and colored glasses are designed and integrated to the laser micromachining system. The cabin system can be seen in Figure 2.8..

Figure 2.8: Isolation Cabin of Laser Micromachining System

Figure 2.9: Laser Micromachining System

Granite based vibration absorber table and isolation cabin with other parts of laser micro manufacturing system are presented in Figure 2.8. Granite based table is placed inside the cabin system as in Figure 2.9.

## 2.4 Cooperation of Devices

Cooperation of devices is another aspect of integration of laser micro machining systems. In order to have a laser micromachining system, positioning and laser systems must communicate and work together. To achieve this cooperation, they are controlled with a multi input controller and forced to use the same interface. In order to achieve cooperation between our positioning and laser system, we used an external communication protocoles, software and hardwares. DB-25 connection type is used for laser control, Labview software and M series NI-SCB 68 DAQ device are used to obtain and manipulate regarding input and outputs.

### 2.4.1 DB-25 Connector

DB-25 connector is being used as a connection type for laser machines by ILDA(International Laser Display Associaton). This protocole is used to connect signal sources to laser projector and it is designed to meet the need of most users. The laser system that is being used in the scope of this study also uses this protocole. This connection type enables to change the intensity of laser beam by changing alignment of active signal ports during the fabrication process. 25 pinout scheme of this connection type is given in Figure 2.10. After necessary investigations, we have succesfully included DB-25 connector to our laser micromachining system.

<table>
<tr><th>PIN No.</th><th>Description</th></tr>
<tr><td>1-8<br>(D0-D7)</td><td>TTL/CMOS levels. Power Setting (0-FFh or 0…255).<br>LSB (D0) corresponds to Pin number 1, MSB (D7) corresponds to pin 8.<br>00h (0): Minimum output power<br>FFh (255): Maximum output power<br>Disconnected corresponds to 00h.</td></tr>
<tr><td>9</td><td>Latch. Latches power setting simultaneously with rising edge.</td></tr>
<tr><td>10-15, 24</td><td>Ground</td></tr>
<tr><td>16, 21</td><td>Laser alarms status.
<table>
<tr><td>Pin 16</td><td>Pin 21</td><td>Status</td></tr>
<tr><td>LOW</td><td>LOW</td><td>Laser temperature is out of operating temperature range</td></tr>
<tr><td>LOW</td><td>HIGH</td><td>Normal operation</td></tr>
<tr><td>HIGH</td><td>LOW</td><td>Laser has automatically switched OFF due to high optical “Back Reflection” returned to the laser</td></tr>
<tr><td>HIGH</td><td>HIGH</td><td>MO failure</td></tr>
</table></td></tr>
<tr><td>17</td><td>Auxiliary 5±0.25VDC power supply for independent guide laser operation.<br>Maximum load current is 0.15A.</td></tr>
<tr><td>18</td><td>Master Oscillator (MO) ON/OFF signal. TTL/CMOS levels.<br>HI: MO ON<br>LOW or disconnected: MO OFF</td></tr>
<tr><td>19</td><td>Laser Modulation input (Power Amplifier ON/OFF input). TTL/CMOS levels.<br>HI: PA ON<br>LOW or disconnected: PA OFF</td></tr>
<tr><td>20</td><td>Pulse Repetition rate (Synchronization) input<br>TTL/CMOS levels square wave. Refer to the specification for operating PRR range.<br>Duty cycle in the range from 0.1 to 0.9.</td></tr>
<tr><td>22</td><td>Guide Laser (red diode) ON/OFF input. TTL/CMOS levels.<br>HI or disconnected: ON<br>LOW: OFF</td></tr>
<tr><td>23</td><td>Emergency Stop Input<br>HI: OK (Normal operation)<br>LOW or disconnected: STOP (Laser automatically switches OFF)</td></tr>
<tr><td>25</td><td>Laser output power monitor (average power).<br>Current loop 4-20mA, recommended load is 200 Ohm.<br>Calibration: 4mA=0W, 10mA=Maximum power.</td></tr>
</table>

Figure 2.10: DB-25 Connector Pin Out Schema [21]

### 2.4.2 NI DAQ and Labview Integration

To cooperate laser and positioning devices, first step is to control them seperately. Hexapod system has a powerful and open source controller and enables inserting new instruments. Controller of the laser system is not capable of adjusting the laser systems power during a fabrication process. In order to overcome this challenge, a new control priciple for the laser system is required. By the help of DB-25 connection type, an M series NI-SCB 68 DAQ device is connected to the main PC with a 25 pinned cable which is produced for DB-25 connector. After that, controller of laser system is deactivated and an user interface is designed to control DAQ device externally.

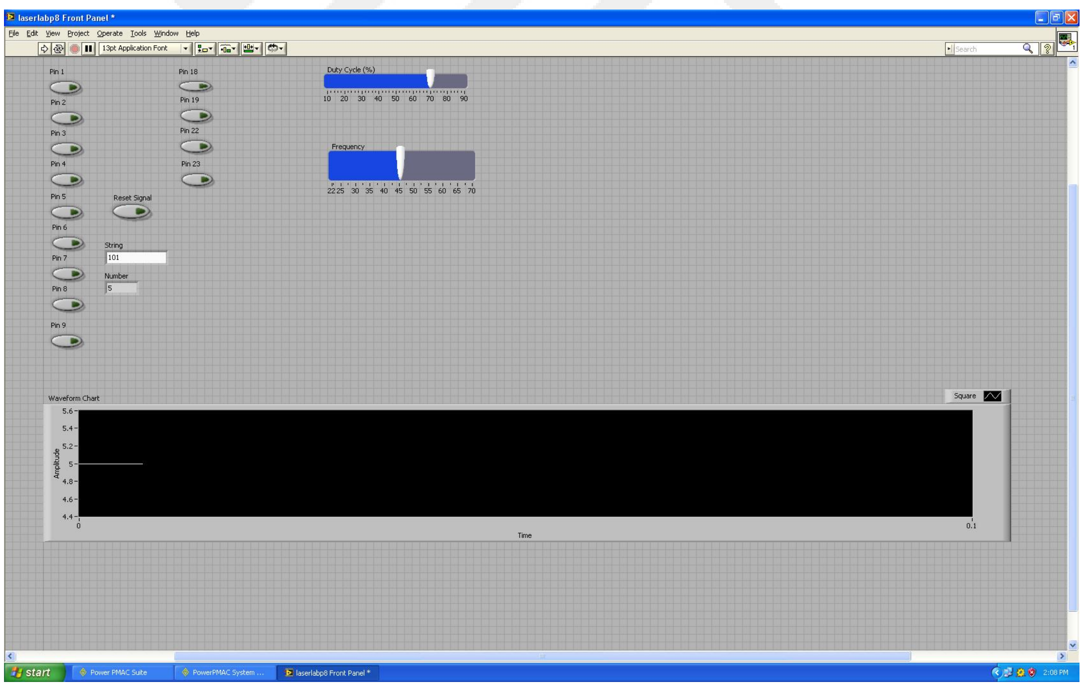


Figure 2.11: Labview Interface 1

Now, this setup enables to use the laser system more effectively. It is possible to obtain regarding input and outputs by the help of M series NI-SCB 68 DAQ and labview interface. By using DB-25 connection schema presented in Figure 2.10 and activating desired pins of this connector, laser systems power can be changed during a fabrication process. In Figure 2.11, Figure 2.12 and Figure 2.13, basic interfaces and cable connections with the instruments are presented.

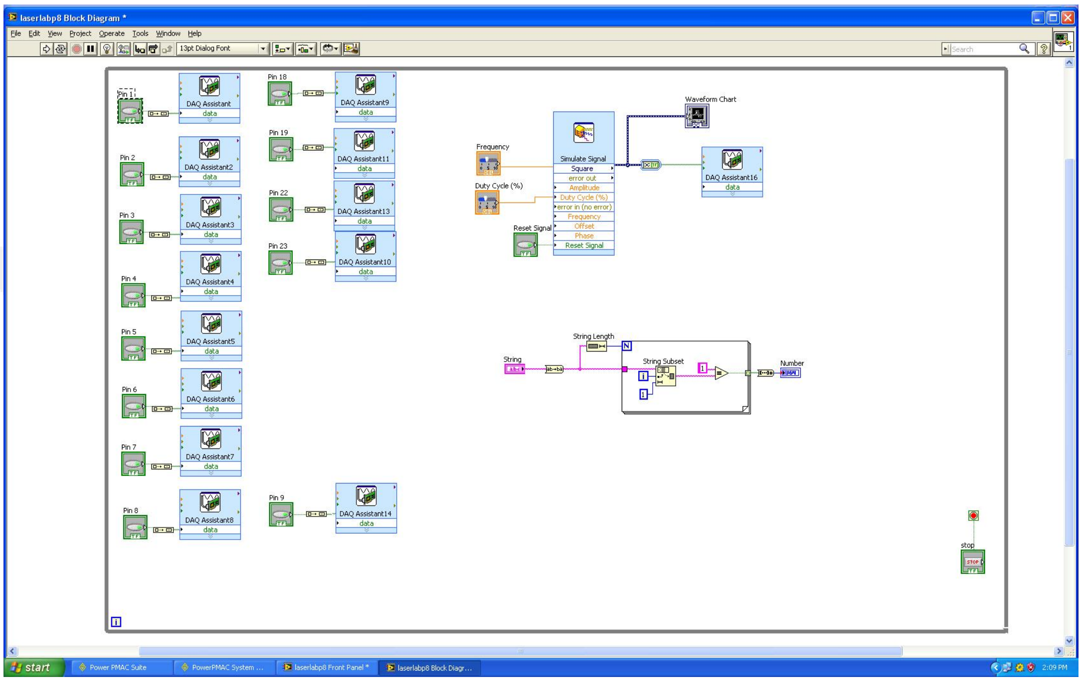


Figure 2.12: Labview Interface 2

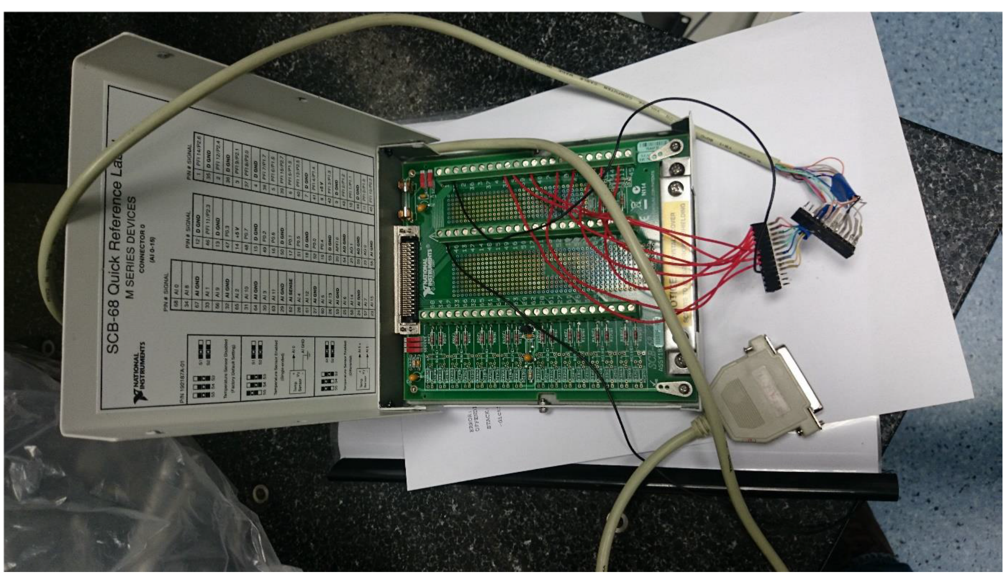


Figure 2.13: NI-SCB 68 DAQ Device

## 2.5 Validation-Calibration Experiments for Laser MicroMachining System

This section presents calibration and validation studies for the laser micromachining system. Laser micromachining system is composed of several parts and these parts originally work independently. After finishing necessary assembling and connections, the next step is to make individual systems work together in an efficient manner. First of all, physical problems like coincidence of coordinate systems of laser and positioning system must be solved. Also, optical lens of laser system is changed which influences spot size, focal length and intensity of the laser system. In order to understand the influence of changes and make these individual components work together, some calibrations and validations must be done.

Initially, laser and positioning systems are assembled to work in same coordinate frame. This issue is solved by both special design of vibration absorber table and assembling the systems on the table. Additionally, an aluminum piece is designed for perfection of the calibration and deviation of coordinate systems which is calculated while both system are working.

Second part of this section is about calibration of the new spot size of the laser system. As reported earlier, optical lens of the laser system is changed in order to achieve desired fabrications with our laser micromachining system. As a first step of calibration of laser system with the overall laser micromachining system, focal length experiments are done.

Another part of the calibration is the experimental intensity investigation. Desired manufacturing studies which are planned with laser micromachining system are on aluminum material. This criteria forced us to change our experimental laser power from 1 to 9 percent.

Final step of calibration is getting new spot size of laser system. Initial spot size of the laser system is about 70 - 80 microns and after changing optical lens from 160mm to 56 mm spot size is decreased about 10 microns.

Some experimental results are given in Figure 2.14 and Figure 2.15. These two experimental results are obtained by testing the new spot size of the system and calibration power parameter for a desired Aluminum sheet material. They are performed with fixed velocity and frequency parameters and a variable power parameter. In Figure 2.13 and 2.15 coincidence of Seg. 1 and Horz. dist. sections of the tables show resultant spot sizes for given parameters. Results of these two experiments show that, spot size is lowered downto 10 micros from 70-80 micros with new optical lens.

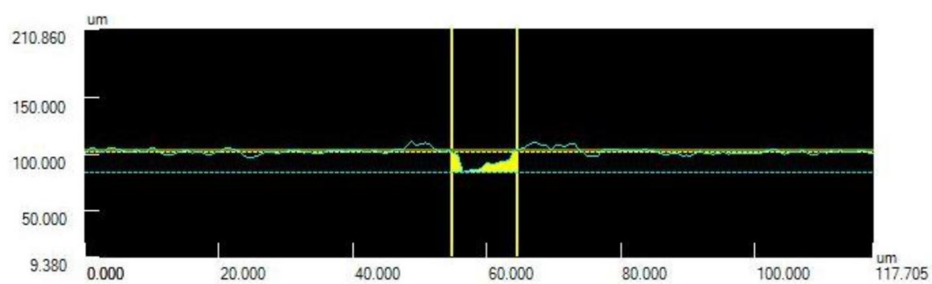


| Profile1 | Horz. dist. | Hght. diff. | Hght. ave. | Angle | C.S. length | C.S. area | R | Comment |
|---|---|---|---|---|---|---|---|---|
| All | 117.705um | 0.455um | 102.190um | 0.221° | 295.316um | 1943.864u... | | |
| Seg.1 | 9.716um | 2.112um | 93.232um | 12.262° | 44.169um | 93.643um2 | | |

Figure 2.14: Spot Size Experiment Results - Power 1 Percent

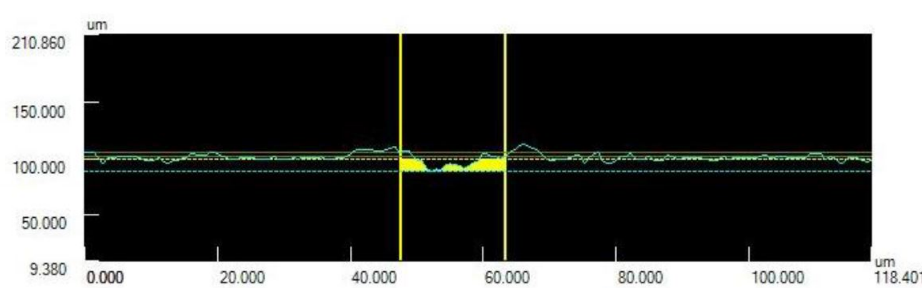


| Profile1 | Horz. dist. | Hght. diff. | Hght. ave. | Angle | C.S. length | C.S. area | R | Comment |
|---|---|---|---|---|---|---|---|---|
| All | 118.401um | 6.750um | 101.392um | 3.263° | 327.391um | 1234.405u... | | |
| Seg.1 | 15.701um | 3.980um | 97.974um | 14.225° | 57.777um | 122.056um2 | | |

Figure 2.15: Spot Size Experiment Results - Power 9 Percent

## 2.6 Manufactured Parts

As mentioned before, we have manufactured various parts with our laser micromachining system. Some of these parts are manufactured for testing the laser micromachining system performance on nonlinear contoured surfaces and for some ongoing projects. Software of the hexapod system allows us to write new motion programs. This property is used to manufacture parts with desired shapes. Figure 2.16 and Figure 2.17 present one of the completed study on a sheet aluminum (100microns thickness) with a non-linear surface. Square holes are created on the surface by the laser system and the move model is developed in a motion program.

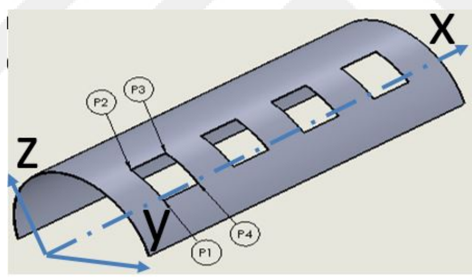


Figure 2.16: Drawing of Manufactured Cylindrical Aluminum Sheet

Figure 2.17: Nonlinear Contour Texturing on a Cylindrical Aluminum Sheet

The Material which is presented in Figure 2.18, is manufactured in the scope of an ongoing project. It is a copper material and laser micromachining system parameters are tuned for this material after performing some experiments and the desired part manufactured.

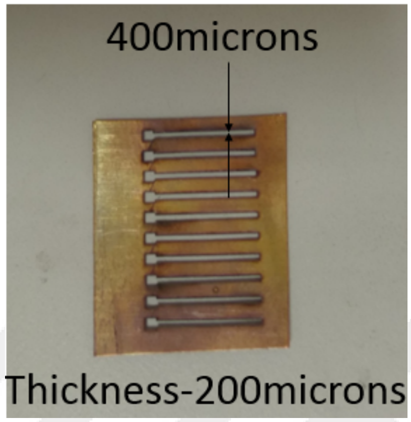


Figure 2.18: Manufactured Copper Plate

Figure 2.19 and Figure 2.20 are taken from a surface texturing study on a nonlinear contoured surface. Figure 2.19 clearly shows the working principle of the laser micromachining system. Laser machine sends the laser beam to the work piece which is fixed on the positioning system. After the process is completed in Figure 2.19, a pattern is created on the surface of the cylindrical material which is presented in Figure 2.20.

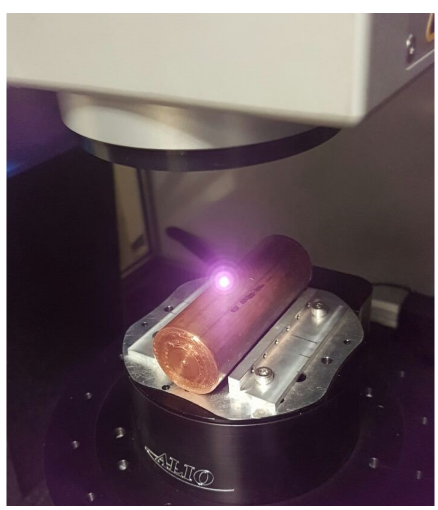

Figure 2.19: Nonlinear Contour Texturing Process

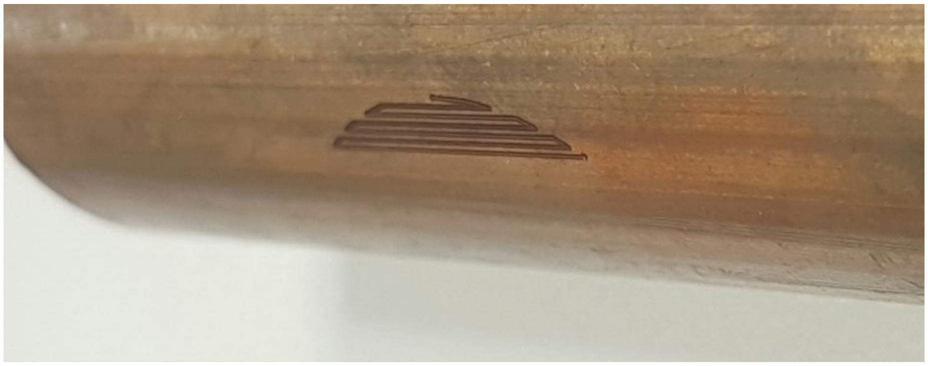

Figure 2.20: Textured Material

After manufacturing presented components, validation and calibration studies are completed for the established laser micromachining system.

To sum up, proposed laser micromachining sytem is establihed successfully. Components of the overall system are dicussed in detail and presented with explanations in the scope of this chapter. Performed validation and calibration tests are also presented with some results. At the end, some manufactured workpieces are illustrated in last section of this chapter with presenting the working principle of the established laser micromachining system.

In order to investigate performance and behaviour of the positioning system, kinematic analysis are performed for the positioning system and they are presented in the following chapter. Besides, a model of the positioning system is created in SimMechanics software by the help of SolidWorks and Matlab environments which are also discussed in the following chapter.

# Chapter 3

# Kinematic Analysis and SimMechanics Model of The Positioning System

Up to this chapter, establishment studies for the developed laser micromanufacturing system is discussed with its components and validation and calibration studies. Also, improvements on laser system and some manufactured workpieces are presented. For further improvements, we directed our studies on the positioning system. In this chapter, performed kinematic analysis of the positioning system are presented. Initially, a detailed description of the manipulator is discussed and hybrid structure of the manipulator explained. After describing the manipulator, inverse and forward kinematics of the positioning system is performed for each path which are explained in hybrid case. At the end of the kinematic analysis, kinematics of each part of the hybrid system composed and presented as whole manipulator. Finally, SimMechanics model of the positioning system is presented and discussed in detail.

## 3.1 Manipulator Description and Kinematics Analysis

The manipulator that we use for precise positioning in laser micromachining system, has six degrees of freedom with a hybrid structure. A hybrid manipulator is a composition of serial and parallel kinematic structures. These structures associate the advantages of both serial and parallel positioning systems in one single structure. Serial part of the positioning system provides a wide work space and the parallel part, which is a 3-RPS parallel manipulator, increases precision of the positioning system.

Due to the hybrid structure of the positioning system, we perform structural analysis for parallel and serial components seperately. These analysis will be integrated and presented at the end of the chapter, so that the kinematic and dynamic analysis of the positioning system become more reliable and understandable. First of all, parallel maipulator part of the system is considered. It constitutes the upper side of the overall manipulator which is a 3-RPS parallel positioning system. A 3-RPS parallel manipulator has three limbs which are composed of Revolute-Prismatic-Spherical(RPS) joints. In serial positioning case, two sliders under the 3-RPS parallel manipulator and a single rotational actuator on the end effector of the overall manipulator are considered.

A 3-RPS parallel positioning system adds three degrees of freedom to the overall system.They are two rotational and one translational motions(rotations are about X and Y axes and translation about Z axis). On the other hand, stages under 3-RPS parallel manipulator and the rotational actuator at the top of the overall system add three more degrees of freedom to the positioning system. These additional freedoms are two translational freedom in X and Y axes and a rotational motion about Z axis. Consequently, the overall positioning system has six degrees of freedom.

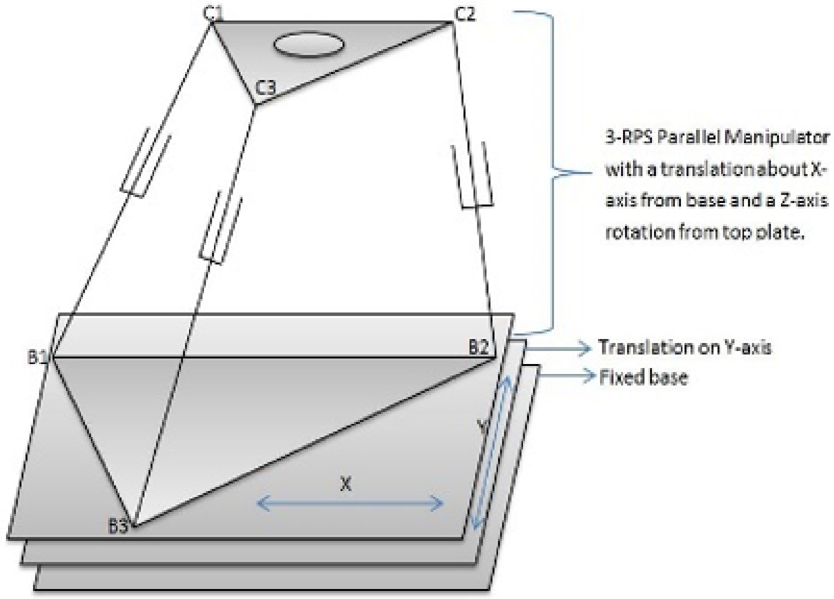


Figure 3.1: Sketch of Hybrid Manipulator

A basic sketch of this positioning system is presented in Figure 3.1. $B_i$ and $C_i$ points on Figure 3.1 are located at revolute and spherical joints of the 3-RPS parallel manipulator. Also, other structural properties are illustrated in this figure. Initially, 3-RPS parallel manipulator will be taken into account for kinematic analysis.

### 3.1.1 Inverse Kinematics

Position analysis of the tool center point (end effector) of a manipulator requires solving forward and inverse kinematics of the positioning system. Inverse and forward kinematics analysis can be done by investigating relations between joints space and cartesian space of the positioning system. Inverse kinematics solution of a positioning system provides joint parameters of the system by using desired position of the end effector. In this part of the study, inverse kinematics of the 3-RPS parallel manipulator will be discussed.

Schematic illustration of the 3-RPS parallel manipulator is presented by Figure 3.2 and Figure 3.3. Three coordinate systems are placed at some necessary points on the manipulator. These points are, at the center of the moving platform($O_1$), at the bottom of the 3-RPS($O_2$) and finally at the bottom of the whole system($O_3$) respectively. Vectoral relations between these coordinate systems and spherical joints of the system are presented in Figure 3.3.

In Figure 3.3, $\vec{r}$ is the position vector of the end effector of the positioning system with respect to $O_2$ coordinate frame. This vector also relates coordinate frames $O_2$ and $O_3$ for translational motion on X, Y and Z axes. $\vec{R}$ is the position vector of the end effector of the positioning system with respect to $O_1$ coordinate frame and represents translational motion of overall manipulator on X, Y and Z axes. $\vec{S}$is a position vector that relates coordinate frames $O_1$ and $O_2$ and it represents translational motions X and Y axes of serial component of the manipulator. $\vec{q_i}$ relates coordinate frame $O_2$ and $\vec{C_i}$ and they are position vectors of spherical joints on the moving platform. $h_1, h_2$ and $h_3$ are the constant offsets on Z-axis between linear actuators at the bottom of the positioning system. $\vec{r}$, $\vec{R}$ and $\vec{S}$ vectors can be presented respectively,

$$\vec{r} = \begin{pmatrix} r_x & r_y & r_z \end{pmatrix}^T, \quad \vec{R} = \begin{pmatrix} R_x & R_y & R_z \end{pmatrix}^T, \quad \vec{S} = \begin{pmatrix} S_x & S_y & S_z \end{pmatrix}^T \tag{3.1}$$

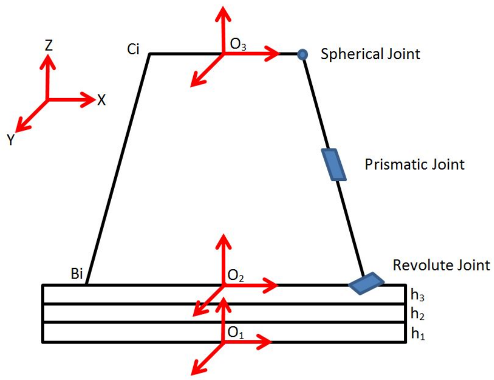


Figure 3.2: Sketch of the Manipulator in Case of Coordinate Systems

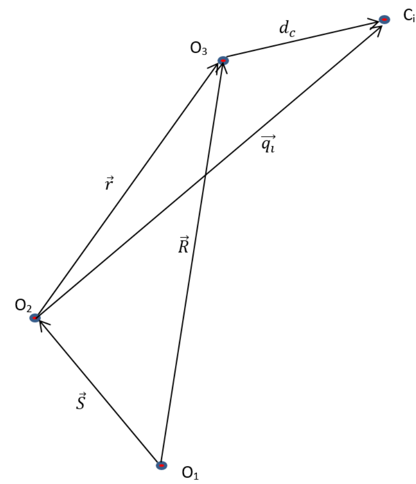


Figure 3.3: Position Vectors between Coordinate Systems and Spherical Joints

By the help of geometrical properties presented in Figure 3.4, vectoral relations between spherical joints and $O_3$ coordinate frame can be obtained as in Eqn. 3.2. $\vec{C_1}, \vec{C_2}$ and $\vec{C_3}$ represent position vector of $C_i$ points with respect to $O_3$ coordinate frame where $d_c$ is the distance between $O_3$ and Ci.

$$\vec{C_1} = \begin{pmatrix} d_c \\ 0 \\ 0 \end{pmatrix}, \vec{C_2} = \begin{pmatrix} -0.5d_c \\ \frac{d_c\sqrt{3}}{2} \\ 0 \end{pmatrix}, \vec{C_3} = \begin{pmatrix} -0.5d_c \\ -\frac{d_c\sqrt{3}}{2} \\ 0 \end{pmatrix} \tag{3.2}$$

Vectoral relations between revolute joints and $O_2$ coordinate frame can be obtained by Eqn. 3.3. $\vec{B_1}, \vec{B_2}$ and $\vec{B_3}$ represent position vector of $B_i$ points with respect to $O_2$ coordinate frame where $d_b$ is the distance between $O_2$ and $B_i$.

$$\vec{B_1} = \begin{pmatrix} d_b \\ 0 \\ 0 \end{pmatrix}, \vec{B_2} = \begin{pmatrix} -0.5d_b \\ \frac{d_b\sqrt{3}}{2} \\ 0 \end{pmatrix}, \vec{B_3} = \begin{pmatrix} -0.5db \\ -\frac{d_b\sqrt{3}}{2} \\ 0 \end{pmatrix} \tag{3.3}$$

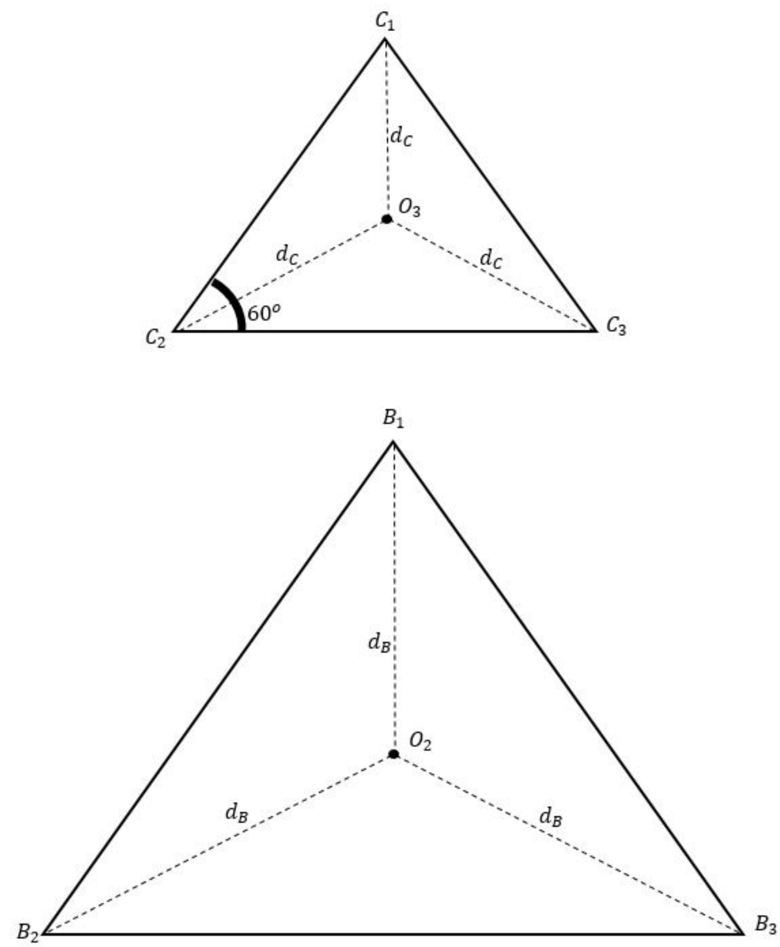


Figure 3.4: Upper and Lower Equilateral Triangles with Geometrical Properties

#### 3.1.1.1 Rotation Matrix

Rotation matrices are used for performing rotations in Euclidean space and they can be used in coordinate transformations. In the case of transformation, rotation matrices transform rotational changes of a coordinate system to another desired coordinate system. For transformation calculations between $O_2$ and $O_3$ coordinate frames of 3-RPS manipulator, a rotation matrix ($R_{BC}$) is used. Due to the geometrical properties of the positioning system the euler sequence of the transformation is choosen as [3, 1, 2]. [22] ,

$$R_{BC} = \begin{bmatrix} u_x & v_x & w_x \\ u_y & v_y & w_y \\ u_z & v_z & w_z \end{bmatrix} \tag{3.4}$$

where u, v and w are direction cosines, and $R_{BC}$ is given as

$$R_{BC} = \begin{bmatrix} \text{c}(\gamma)\text{c}(\alpha)\text{+ s}(\alpha)\text{s}(\beta)\text{s}(\gamma) & \text{-c}(\gamma)\text{s}(\alpha)\text{+ c}(\alpha)\text{s}(\beta)\text{s}(\gamma) & \text{c}(\beta)\text{s}(\gamma) \\ \text{c}(\beta)\text{s}(\alpha) & \text{c}(\beta)\text{c}(\alpha) & \text{-s}(\beta) \\ \text{-s}(\gamma)\text{c}(\alpha)\text{+ c}(\gamma)\text{s}(\beta)\text{s}(\alpha) & \text{s}(\gamma)\text{s}(\alpha)\text{+ c}(\alpha)\text{s}(\beta)\text{c}(\gamma) & \text{c}(\beta)\text{c}(\gamma) \end{bmatrix} \tag{3.5}$$

In $R_{BC}$ matrix, $\alpha$, $\beta$ and $\gamma$ are Euler angles and s($\alpha$) = sin($\alpha$) and c($\alpha$) = cos($\alpha$).

Now, by using above equations, position vectors of spherical joints can be calculated with respect to $O_2$ coordinate frame and scalar value of limb lenghts for 3-RPS parallel manipulator can be derived as,

$$\vec{q_i} = R_{BC}{}^{O_3}\vec{C_i} \tag{3.6}$$

$$L_i = norm[\vec{r} + \vec{q_i} - \vec{B_i}] \tag{3.7}$$

where ${}^{O_3}\vec{B_i}$ and ${}^{O_3}\vec{C_i}$ are representation of $\vec{B_i}$ and $\vec{C_i}$ vectors with respect to $O_3$ coordinate frame.

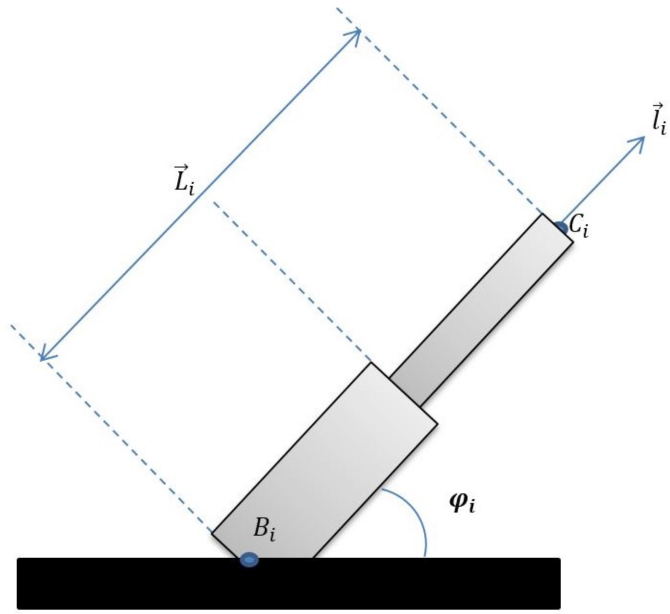


Figure 3.5: Limb Lenght and Angle $\varphi_i$ Illustration on a Chain of 3-RPS

In Figure 4.4, limb angle $\varphi_i$ and limb length $L_i$ of a link of 3-RPS parallel manipulator are illustrated. $\varphi_i$ 's are the angles between the plane on coordinate system $O_2$ and links.

### 3.1.2 Forward Kinematics

Forward kinematics solution of a positioning system provides position of end effector of the system by using specified joint parameters. For specified 3-RPS parallel manipulator, limb angle $\varphi_i$ and limb length $L_i$ are joint parameters. Solution of forward kinematicswill be helpful for both checking the solutions of the inverse kinematics and trajectory tracking studies.

$$\vec{l_1} = \begin{pmatrix} \cos(\varphi_1) & 0 & \sin(\varphi_1) \end{pmatrix}^T \tag{3.8}$$

$$\vec{l_2} = \begin{pmatrix} \text{-}\cos(\varphi_2)/2 & \cos(\varphi_2)\sqrt{3}/2 & \sin(\varphi_2) \end{pmatrix}^T \tag{3.9}$$

$$\vec{l_3} = \begin{pmatrix} \cos(\varphi_1) & \text{-}\cos(\varphi_2)\sqrt{3}/2 & \text{-}\sin(\varphi_2) \end{pmatrix}^T \tag{3.10}$$

$$\vec{L_1} = \vec{l_1} L_1 \tag{3.11}$$

$$\vec{L_2} = \vec{l_1} L_2 \tag{3.12}$$

$$\vec{L_3} = \vec{l_1} L_3 \tag{3.13}$$

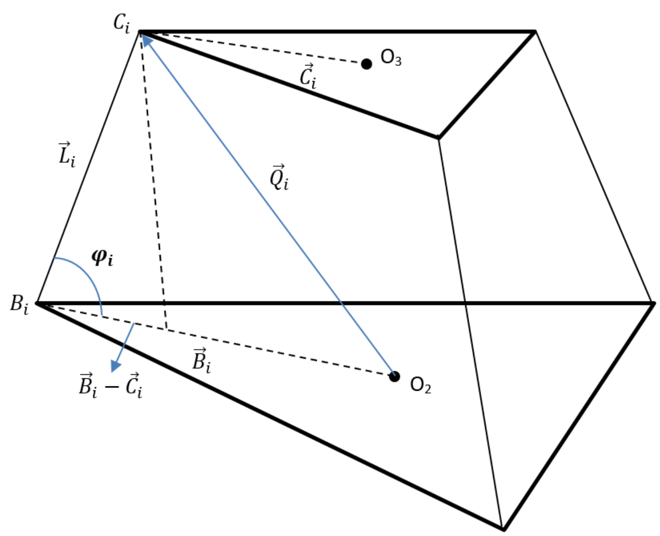


Figure 3.6: Position Analysis for Spherical Joints

Vectors $\vec{l_1}$, $\vec{l_2}$ and $\vec{l_3}$ are the unit vectors that represent direction of each leg and $\vec{L_1}$, $\vec{L_2}$ and $\vec{L_3}$ are vectors of legs. Leg vectors can be found by multiplying unit leg vectors with leg lenghts. Derivation of these parameters are given from Eqn. 3.8 to Eqn. 3.13 After that, Eqn. 3.14 can be derived to find the positions of spherical joint coordinates with respect to $O_2$ coordinate system. Relations are illustrated on Figure 3.6.

$${}^{O_2}\vec{C_i} = {}^{O_2}\vec{B_i} - L_i cos(\varphi_i) + L_i sin(\varphi_i) \tag{3.14}$$

Notice that, $^{O_2}\vec{C_i}$ is the representation of $\vec{q_i}$ with joint parameters $\varphi_i$'s and $L_i$'s instead of cartesian space parameters. They are the position vectors between $O_2$ coordinate frame and the centers of the spherical joints. They are on the edges of the moving platform which are the corners of an equilateral triangle that is presented in Figure 3.4. Let us use $\vec{Q_i}$ in order to $^{O_2}\vec{C_i}$ for simplification of future calculations. Consequently, we can use Eqn. 3.15 to find the cartesian coordinates of the end effector.

$$\vec{Q_c} = \frac{\vec{Q_1} + \vec{Q_2} + \vec{Q_3}}{3} \tag{3.15}$$

$\vec{Q_c}$ is the xyz cartesian coordinates of the end effector. Nonlinear equations are given in Eqn. 3.16 to 3.18 are the relations between limb lenghts and angles $\varphi_i$'s. They are solved numarically by fsolve comment which is a nonlinear equation solver in Matlab. By using these equations, $\varphi_i$'s can be obtained numerically to be used as inputs of forward kinematics equations. After that, forward kinematic analysis can be performed.

$$f_1(\varphi_1,\, \varphi_2,\, L_1,\, L_2) = (\tfrac{L_1}{d_b})^2 + (\tfrac{L_2}{d_b})^2 + 3 - 3(\tfrac{d_c}{d_b})^2 + (\tfrac{L_1}{d_b})(\tfrac{L_2}{d_b})\cos(\varphi_1)\cos(\varphi_2) -$$
$$2(\frac{L_1}{d_b})(\frac{L_2}{d_b})sin(\varphi_1)sin(\varphi_2) - 3(\frac{L_1}{d_b})cos(\varphi_1) - 3(\frac{L_2}{d_b})cos(\varphi_2) = 0 \tag{3.16}$$

$$f_2(\varphi_2,\, \varphi_3,\, L_2,\, L_3) = (\tfrac{L_2}{d_b})^2 + (\tfrac{L_3}{d_b})^2 + 3 - 3(\tfrac{d_c}{d_b})^2 + (\tfrac{L_2}{d_b})(\tfrac{L_3}{d_b})\cos(\varphi_2)\cos(\varphi_3) -$$
$$2(\frac{L_2}{d_b})(\frac{L_3}{d_b})sin(\varphi_2)sin(\varphi_3) - 3(\frac{L_2}{d_b})cos(\varphi_2) - 3(\frac{L_3}{d_b})cos(\varphi_3) = 0 \tag{3.17}$$

$$f_3(\varphi_1,\, \varphi_3,\, L_1,\, L_3) = (\tfrac{L_1}{d_b})^2 + (\tfrac{L_3}{d_b})^2 + 3 - 3(\tfrac{d_c}{d_b})^2 + (\tfrac{L_1}{d_b})(\tfrac{L_3}{d_b})\cos(\varphi_1)\cos(\varphi_3) -$$
$$2(\frac{L_1}{d_b})(\frac{L_3}{d_b})sin(\varphi_1)sin(\varphi_3) - 3(\frac{L_1}{d_b})cos(\varphi_1) - 3(\frac{L_3}{d_b})cos(\varphi_3) = 0 \tag{3.18}$$

By computing $\varphi_i$'s and $\vec{L_i}$'s from kinematic analysis, we can now obtain rotational position of the upper platform of 3-RPS parallel manipulator. By using rotation matrices given in Eqn. 3.4 and Eqn. 3.5, the direction cosines ($\vec{u}$, $\vec{v}$ and

$\vec{w}$) can be found and related angles can be obtained. Solutions of Eqn. 3.19 to 3.24 gives the direction cosines as follows,

$$\vec{u} = \begin{pmatrix} u_x & u_y & u_z \end{pmatrix}^T \tag{3.19}$$

$$\vec{v} = \begin{pmatrix} v_x & v_y & v_z \end{pmatrix}^T \tag{3.20}$$

$$\vec{w} = \begin{pmatrix} w_x & w_y & w_z \end{pmatrix}^T \tag{3.21}$$

$$\vec{u} = (\vec{Q_1} - \vec{Q_c})/\vec{C_1}(1) \tag{3.22}$$

$$\vec{v} = (\vec{Q_2} - \vec{Q_3})/(\vec{C_2}(2) - \vec{C_3}(2)) \tag{3.23}$$

$$\vec{w} = \vec{u} \times \vec{v} \tag{3.24}$$

Solutions of euler angles can be obtianed by Eqn. 3.25 - Eqn. 3.27 as follows,

$$\alpha = \arctan(\vec{w_x}/\vec{w_z}) \tag{3.25}$$

$$\beta = \arctan(\vec{u_y}/\vec{v_y}) \tag{3.26}$$

$$\gamma = \arcsin(-\vec{w_y}) \tag{3.27}$$

Solution of three rotational motions are represented in previous equations and solution of translational motions can be obtained by using $\vec{Q_c}$ which is the xyz coordinates of the tool center point. $\vec{Q_c}$ is a 3x1 vector where X, Y and Z axes are first, second and third rows of this vector respectively.

$$X = Q_c(1) \tag{3.28}$$

$$Y = Q_c(2) \tag{3.29}$$

$$Z = Q_c(3) \tag{3.30}$$

Now, kinematic solutions of serial components of the overall positioning system can be added to kinematics of 3-RPS manipulator. Rotations about X ($\alpha$) and Y ($\beta$) axes and translation in Z axis are found with Eqn 3.25, Eqn 3.26 and Eqn 3.30 for 3-RPS parallel manipulator respectively. Remaining three defrees of freedom are not fully independent from previous calculations. In the next step, these solutions will be combined with the following analysis.

positioning system have three more actuation systems for remaining motions which are translational motions about X and Y axes and a rotational motion about Z axis ($\gamma$). In order to find exact positions on the remaining axes, X and Y axes positions of 3-RPS parallel manipulator will be added to actuator positions on these axes. 3-RPS positioning system does not have any effect on rotation $\gamma$. So, only a rotational and independent actuator will be used for this rotational motion.

Lets define Px and Py for actuator positions on X and Y axes and use $\gamma_a$ to define to attain actuator position for rotational motion about Z axis. Finally, remaining three degrees of freedom can be obtained by using following relations.

$$X = P_x + Q_c(1) \tag{3.31}$$

$$Y = P_y + Q_c(2) \tag{3.32}$$

$$\gamma = \gamma_a \tag{3.33}$$

## 3.2 SimMechanics Model of positioning System

SimMechanics is a simulation software which enables to model three dimesional mechanical systems and it works with Simulink environment. For simulation and control studies, a SimMechanics model is created for the positioning system of laser micromachining system.

First of all, each part of positioning system is modeled in SolidWorks modeling program. After that, modeled parts are assembled with respect to joint properties of manipulator. Next step is adjusting the mating properties of joints according to SimMechanics. Otherwise, with incorrect mating, SimMechanics model cannot be operated correctly. The matings that yield correct joint properties are presented in Figure 3.7, Figure 3.8 and Figure 3.9. Figure 3.7 illustrated mating for spherical joint. A spherical joint has three degrees of freedom in space so it must be mated point to point in SolidWorks. Prismatic joint mates are presented in Figure 3.8. A prismatic joint has one degree of freedom in space and it generates linear motion. In order to have a prismatic joint behaviour, parts shuold be mated with two vertical planes. Eventually, a revolute joint has a rotational degree of freedom in space and components must be mated concentric to obtain a revolute joint.

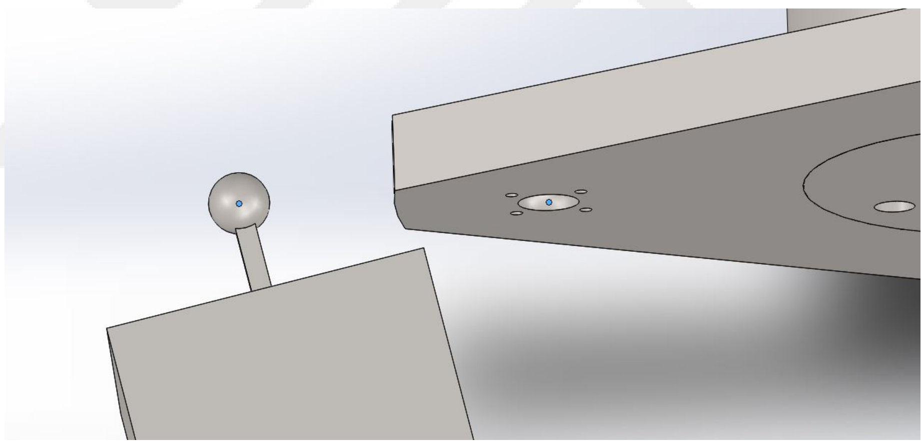

Figure 3.7: Spherical Joint Mating in SolidWorks

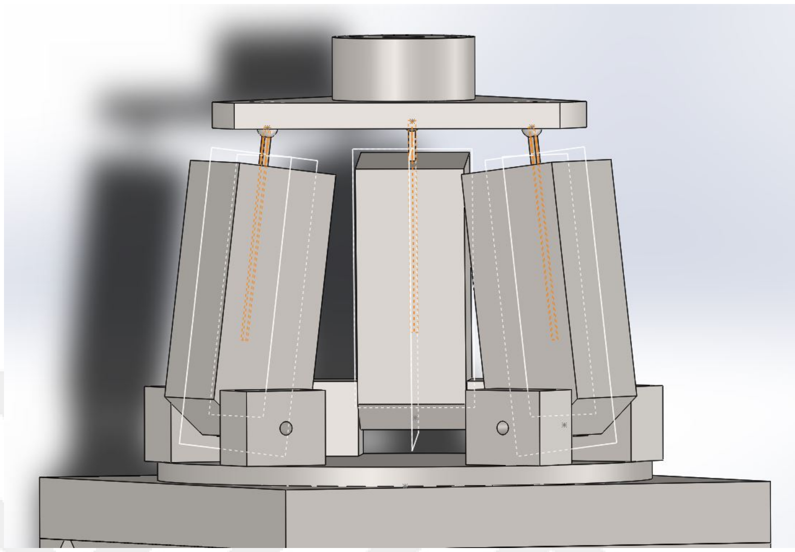

Figure 3.8: Prismatic Joint Mating in SolidWorks

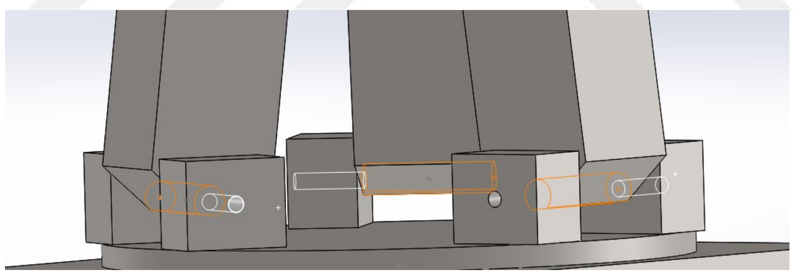

Figure 3.9: Revolute Joint Mating in SolidWorks

Finally, CAD model of the overall positioning system can be imported to SimMechanics environment. A view of imported model is presented in Figure 3.10.

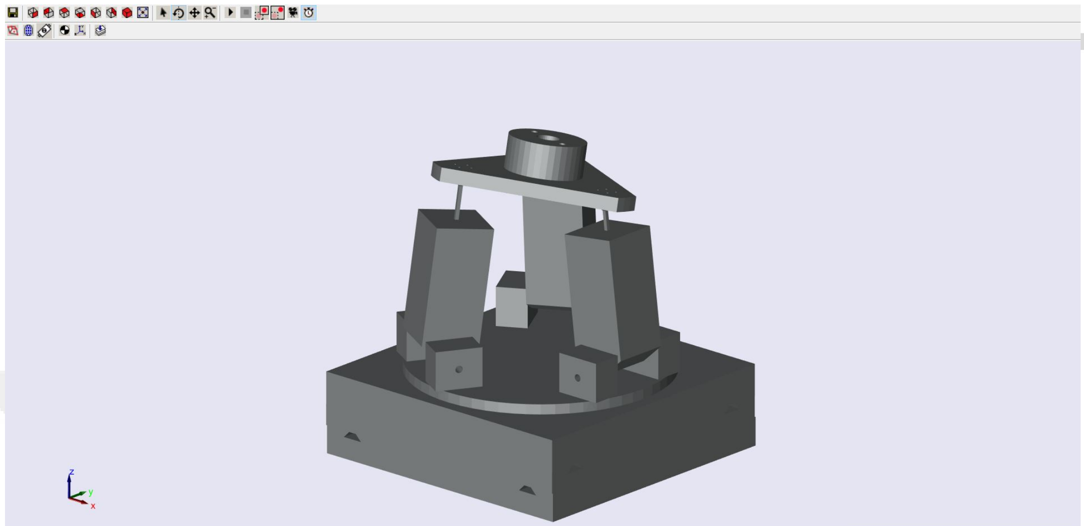

Figure 3.10: View of Overall positioning System Model in SimMechanics

After importing the SolidWorks model to SimMechanics, software creates a block diagram by taking the mating properties of the SolidWorks model into account. Beside, for visualization of simulations, SimMechanics uses imported SolidWorks parts. Block diagram of the imported model enables to make changes in physical properties of the system. Also, as another important contribution of the SimMechanics simulation software, block diagrams provide adding actuators to desired joints and makes possible to perform various simulation studies.

Imported manipulator model can be used as a dynamic model of the positioning system. This can be done by adjusting mass properties of each components and inserting actuators to active joints as in the actual positioning system. The dynamic model will be discussed in detail on following chapters.

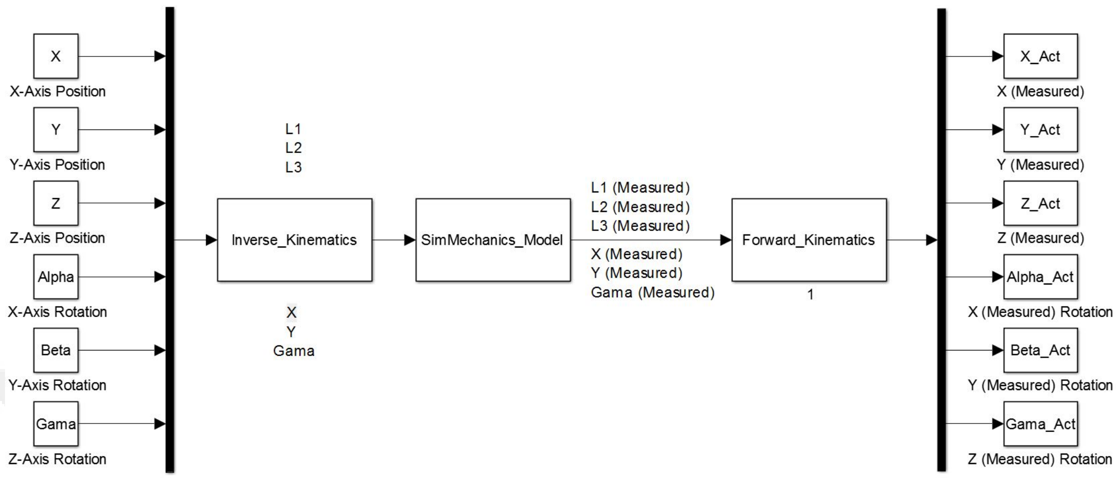


Figure 3.11: Representative Schema of the Manipulator Model

A representative schema of the model of the positioning system is given in Figure 3.11. This schema includes inverse and forward kinematics of the positioning system. To perform trajectory tracking with the manipulator, a trajectory should be generated. According to SimMechanics model the desired trajectory should be converted to joint space from catersian space and this conversion can be done by using inverse kinematics of the positioning system. Simulation model gets desired joint space information of the generated trajectory with its actuators actuators on active joints and creates an measured joint space information as an output of actuators. The created joint space information can be converted to cartesian space and generates an measured trajectory. The difference between measured and desired paths show the trajectory trackig performance of the system which will be discussed in detail on following chapters.

In this chapter, our hybrid positioning system is described and kinematic analysis is performed. This gives us the ability of observing both joint space and cartesian space position informations of the positioning system. A Matlab/SimMechanics model of the positioning system is also presented in this chapter. This model is created to observe dynamic behaviour of the manipulation system for position control studies. Finally, a representative schema of the manipulator model is presented with inverse and forward kinematics to clarify the use of the kinematic analysis and the simulation model. In the following chapter, improvements on the control system of the positioning system will be discussed. In this discussion, performed kinematic analysis and created model which are presented in the scope of this chapter will be used.

# Chapter 4

# Improvements on the Control System of the Manipulator

In the scope of this study, a laser micromachining system is developed and several contributions are implemented. These contributions are intended for improving the performance of the laser micromachining on nonlinear contoured surfaces. First improvement is implemented by changing the original optical lens of the laser system. As a result, spot size of the system decreased from 70-100 micrometers to 10 micrometers. The second improvement is achieved with the power control component of the laser system where the original controller of the laser system is deactivated and laser system is updated with a new power control system. This update added a capability of changinig the power level of the laser system during processes. As a final contribution, investigations are directed to measured manipulator properties. In order to achieve this, kinematic anaylsis are performed and a simulation model for the positioning system is created. These improvements and analysis are performed up to this chapter and further studies on the positioning system will be performed in this chapter.

First of all, performance of the positioning system is tested with a nonlinear trajector and problematic parts are investigated. After that, new controller parameters are tuned for the controllers of both simulation model and actual positioning system by using manual tuning techinque which is also explained in this chapter. Nonlinear trajectory tracking performance of the positioning system directed improvement studies to actuators on limbs of the positioning system. As mentioned in chapter 3, two of three rotational degrees of freedom are added to the overall positioning system by limbs of 3-RPS parallel manipulator.

The trajectory which is used for the experiments and simulations is presented in Figure 4.1. This trajectory includes both translational and rotational motions and it activates most of the actuators of the positioning system. With given path, positioning system uses both serial and parallel manipulator properties of its hybrid structure while tracking it. As can be seen in Figure 4.1, the trajectory has some sharp corners which is considered as a challenge for positioning systems. Besides, for contour texturing experiments it is possible to find various cylindrical workpieces for this kind of trajectory. These are the reasons of usage of this kind of path for our nonlinear performance investigations on the positioning system.

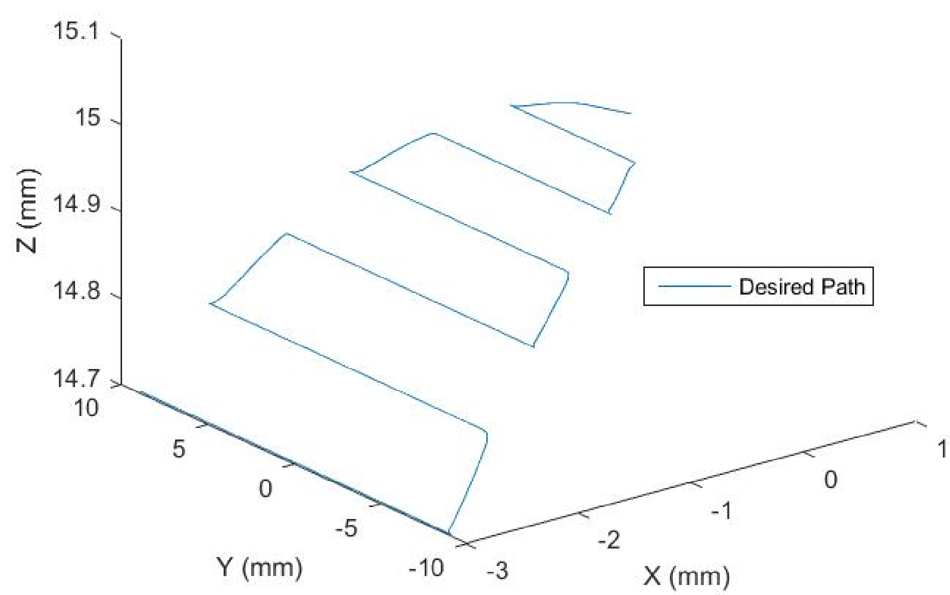


Figure 4.1: Desired Trajectory Which is Uploaded to the Positioning System

The trajectory presented in Figure 4.1 is uploaded to software of the positioning system. Measured and desired actuator position informations are gathered from the encoders of the actuators of the positioning system. By using the forward kinematics of the positioning system, measured actuator informations are converted to measured trajectory tracking informations. Schema of this conversion is presented in Figure 4.4. Examples of the results of this conversion are presented in Figure 4.2 and Figure 4.3. Figure 4.2 compares the desired nonlinear trajectory which is generated for simulation and measured trajectory tracking results of the manipulator. Figure 4.3 illustrates the comparison of measured and desired positions for one limb of the positioning system.

Results which are presented in Figure 4.2 and Figure 4.3, show that there are some errors on trajectory tracking performance of the positioning system. Outcome of the observations on the performance of the actuators and comparison of the measured and desired trajectory tracking performances show that, the performance of the positioning system decreases due to the position tracking performance of the limb actuators.

Positioning system uses PID controllers to minimize the error of positioning by performing a better positioning with its actuators. Measured results, which are presented in Figure 4.2 and Figure 4.3 are obtained with the current PID controller parameters of the positioning systems while performing a nonlinear trajectory tracking performance.

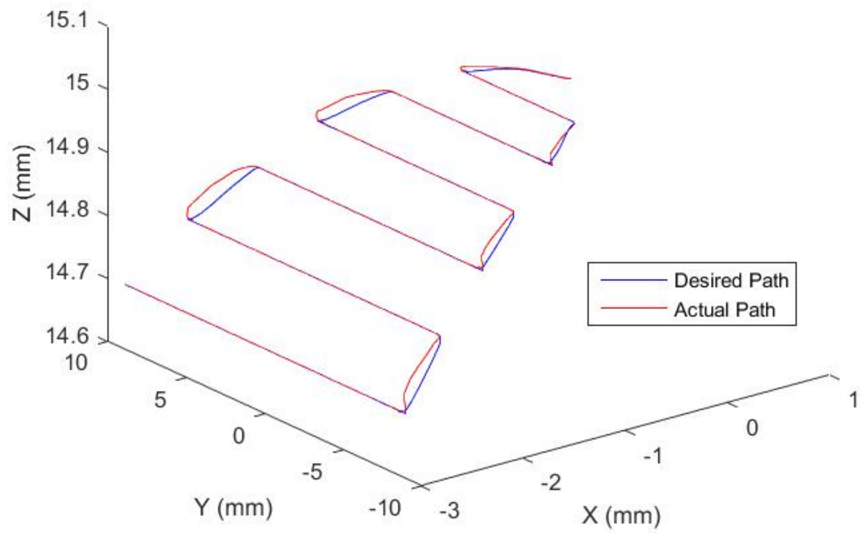


Figure 4.2: Trajectory Tracking Plot of Measured vs Desired Position

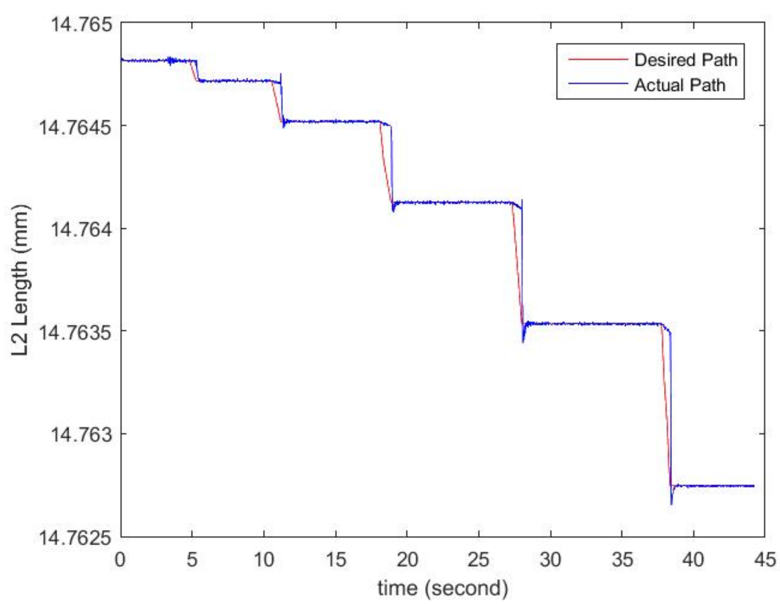


Figure 4.3: Measured vs Desired Position Comparison of a Link Actuator

Positioning system and inverse-forward kinematics relations are decomposed to gather and upload position information of the joint actuators. This decomposition is used to investigate the response of the active actuators and a schema of this decomposition is illustrated in Figure 4.4. This decomposition helps to carry out control studies for the positioning system, since it enables to gather measured and desired trajectory tracking data of the positioning system. Figure 4.2 and Figure 4.3 and other experimental results are obtained by using the schema which is presented in Figure 4.4.

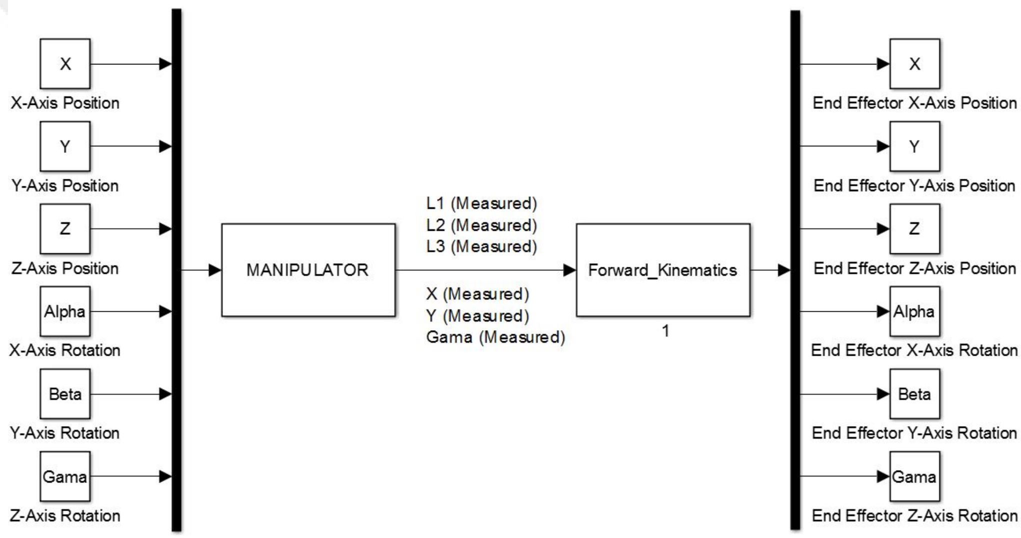


Figure 4.4: Developed System Model

After performing trajectory tracking experiments with the positioning system, performance improvement studies are carried out in two steps. In first step, some simulations are done with Matlab/SimMechanics simulation software with PID controllers and PID control parameters are tuned to minimize the error between measured and desired results of positioning. Then, by using simulation results of SimMechanics model, measured PID parameters of the manipulator controllers are tuned. With tuned PID control parameters, performance of the positioning system is improved for nonlinear trajectory tracking case. Parameter tuning studies are done manually by comparing response of the simulation model and positioning system.

## 4.1 Manual Tuning

PID control parameter tuning can be performed by manually or using some rule based tuning methods. Rule based method have some limitations. For example, they may not support different types of plant models. Manual tuning methods are more effective for online tuning case. They are time consuming, experimetal and iterative techniques and they can cause damage on hardware. [23]

For an online system, manual tuning of PID control parameters can be performed as follows,

- First, set integral ($K_i$) and derivative ($K_d$) gain values zero.

- Increase proportional ($K_p$) gain until the output starts oscillation.

- Use half of the $K_p$ which is used in oscillated state.

- Increase $K_i$ until response reaches around the setpoint.

- Increase $K_d$ in small steps until the observing a quick response.

## 4.2 SimMechanics Position Control Simulations

SimMechanics model of the positioning system is created by using kinematic analysis and SolidWorks model is derived in the scope of this study. This simulation software enables to attain actuation to the desired joints of the manipulator. By using experimental results and kinematic solutions, the actuated joints of the manipulator model is feeded with joint positions. Also, in SimMechanics model, physical properties of the modeled manipulator system can be changed. Mass properties of some parts of the manipulator model are optimized by comparing results of simulations with the measured positioning system. With optimized properties, a dynamic model of the positioning system is obtained in the simulation environment. This dynamic model is fed with the desired position data of the previously generated nonlinear trajectory and the response of the system is investigated. After investigations, PID controllers are implemented to link actuators and then the error of the positioning is observed by using output data of the actuated joints. Actuator position data are converted to end effector position data by using forward kinematics of the positioning system and error of the trajectory tracking performance of the dynamic model is investigated.

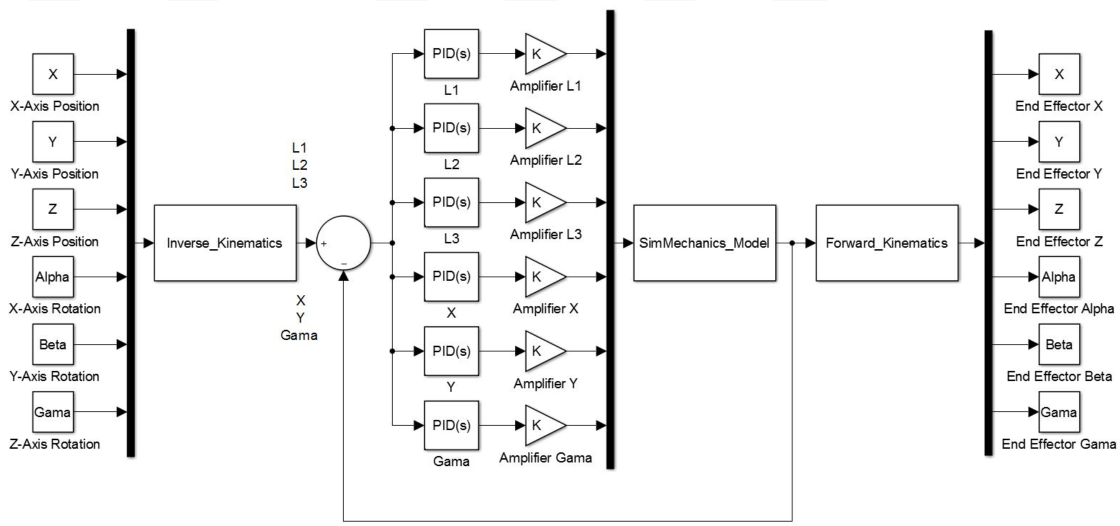


Figure 4.5: Simulation Schema

Control schema of SimMechanics position control simulations is presented in Figure 4.5. Schema includes inverse kinematics, PID controllers and SimMechanics model of the positioning system. Desired position data of the nonlinear trajectory that we have provided is implemented in inverse kinematics solution of the manipulator and the output data of inverse kinematics are joint positions for desired trajectory. Desired joint position data is fed to SimMechanics model and the measured joint position data of the SimMechanics model can be gathered. Gathered data is compared with desired joint position data and the error of the positioning is calculated for each active joint. Then, position error information of active joints are directed to PID controllers of the each active joints, which are attained to actuators of the joints. Finally, Proportional, Integral and Derivative gains of the PID controllers are tuned with respect to position error informations to improve the performance of the manipulator model on nonlinear trajectory tracking. PID control parameter tuning studies are done by manual tuning.

Positioning system is obtained from a commercial company and all specifications are not available. Because of this reason, in SimMechanics and Simulink model, there are some unmodeled parts for the positioning system. For example, mass and inertia properties are not available. However, these properties can be optimized by changing the mass properties in SimMechanics model and geometrical properties of the manipulator should be implemented correctly in SolidWorks. The positioning system has a gravity compensation system by air supply which makes gravitational forces on actuators zero and actuators apply forces in same direction with gravity instead of dealing with gravity. So, the gravity compensation system makes masses of structures zero and the actuators try to apply force to deal with supplied air force which is not important when compared to the real component masses. Gravity compensation of the manipulator simplified the optimization studies for mass properties of the manipulator model.

Another important part for the dynamic model of the manipulator is the amplifiers and actuators on the active joints. There is not enough information about actuator and amplifier properties and it creates problems for the dynamic model of the positioning system. Figure 4.6 presents components of motion control system. According to the schema presented in Figure 4.6, we send position informations to the motion controller and observe the output data of motor without any amplifier and motor informations. This issue influences the results of the simulations. In order to overcome this challenge, some gains are implemented to the model to minimize the behaviour of amplifier and actuator models in Simulink and SimMechanics. These gains are presented in Figure 4.5 and which called Amplifier.

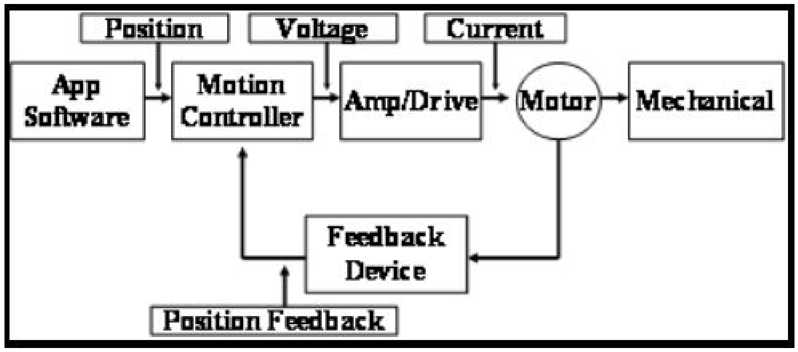


Figure 4.6: Components of a Motion Control System [24]

Optimizations for unmodeled system parameters are achieved by using original manipulator PID controller parameters of positioning system. Comparison of kinematic results of the manipulator and SimMechanics model for a desired trajectory is helped to optimize the unmodeled system parameters. After all optimization and implementations are done for the positioning system model in Simulink and SimMechanics model, we can now start simulations.

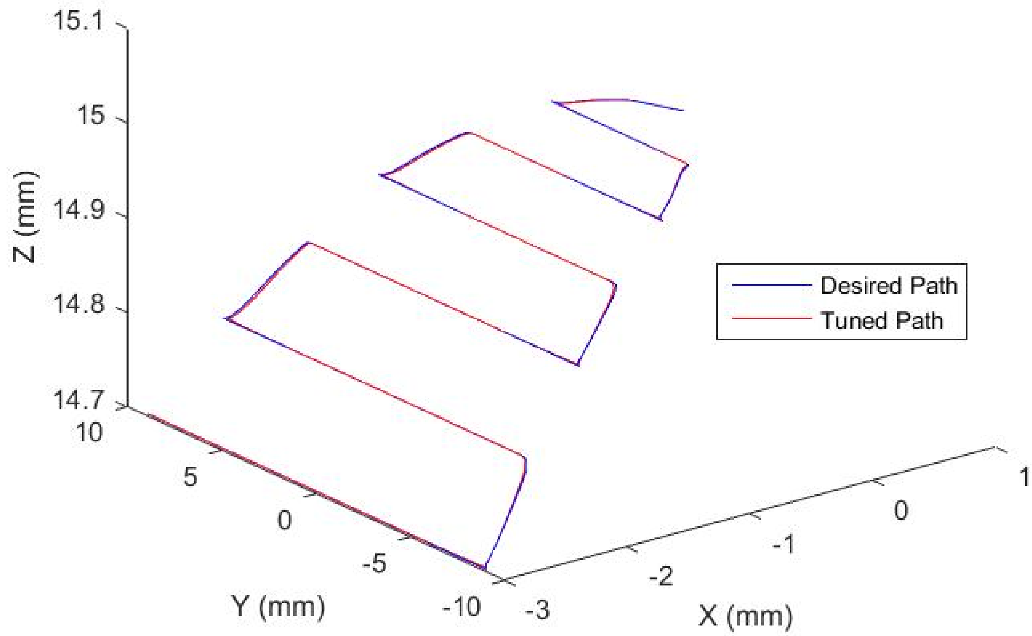


Figure 4.7: Comparisn of Tuned and Desired Trajectory Tracking Results

Finally, simulation results for the best trajectory tracking performance obtained by tuned PID parameters in SimMechanics model of the positioning system. Figure 4.7 shows the desired and tuned trajectory tracking results. Tuned PID parameters are also implemented to the controller of the manipulator and used for experiments.

## 4.3 Tuning the Controller Parameters of the Manipulator

Positioning system uses PID controllers to improve positioning performance. Controller and interface structures of the positioning system enable to change PID control parameters for user. Original control parameters of the system are close to perfect for linear motion case. However, experimental results show that the original controller parameters of the positioning system need to be modified for nonlinear trajectory tracking operations to obtain better result with nonlinear trajectories. Figure 4.2 clearly shows the performance of the positioning system on nonlinear trajectory tracking operations. As a second step of improvement of control system of manipulator for nonlinear trajectory tracking, PID control parameters of the positioning system are tuned experimentally by using user interface of the positioning system.

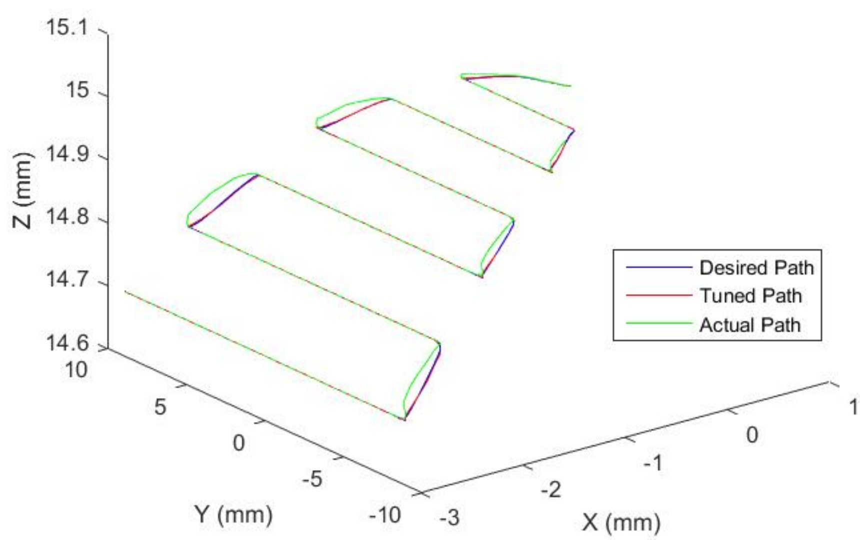


Figure 4.8: Tuned Trajectory Comparison with Measured and Desired Trajectory Tracking Results

Initially, PID control parameters which are obtained by using simulations are implemented to the PID controller on the active joints of the positioning system. Resultant manipulator performance was not good enough and the positioning system was oscillating. So, by using manually tuning technique for PID control parameters, $K_p$ is decreased iteratively and optimum $K_p$ parameter is obtained. Then, $K_i$ and $K_d$ control parameters which are obtained from simulations fit effectively in real positioning system and we did not change them. As a result, only the proportional gain is tuned with the real manipulator experiments and performance of the positioning system for nonlinear motions is improved. The nonlinear trajectory tracking performance results which are presented in Figure 4.7 shows the final tuning performance results of the control system improvement studies on the positioning system.

In this chapter, improvements on the control system of the positioning system described and explained in detail. A desired trajectory which is used in performance test of the positioning system is presented and PID parameter tuning technique is explained clearly. Optimization studies for the simulation model was another consideration of this chapter and it is explained with reasons. After that, strategies for improvements on the control systems of the positioning system and the simulation system are presented with representative schemas. Before and after tuning performance of the actual positioning system and simulation model are also presented with figures in both cartesian and joint space.

In the following chapter, simulation and experimental results of the studies which are performed up to now will be discussed. Control parameter of the actual positioning system and simulation model will be presented with inital and final results.

# Chapter 5

# Simulations and Experimental Results

Results of this thesis are presented in this chapter. Initially, results of spot size and power properties are discussed. Original optical lens of the laser system is changed with a new one to decrease the spot size of the laser. A smaller spot size enables to performe more precise micromachining for laser systems. By changing lens of the laser system, some other properties of the output laser beam are also changed. A major change is occured in the laser power as discussed in previous chapters.

To improve the performance of the laser micromachining system on nonlinear surfaces, nonlinear trajectory tracking performance of the positioning system is investigated. Results of this investigation show that, performance of the manipulator should be improved in order to achieve a better performance in case of nonlinear trajectory tracking. For this purpose, motion programs are generated and uploaded to the positioning system and motor position informations of the manipulator are obtained from encoders of the actuators. By using some softwares and kinematic model of the manipulator, a dynamic model of the positioning system is created and optimized. The dynamic model is used for simulations to improve the performance of the manipulator. For position control studies PID controllers are used as controller for simulations because the actual manipulator uses PID controllers.

Development and optimization of simulation model of the actual positioning system is explained and discussed in detail in the scope of this chapter. Nonlinear trajectory tracking performance comparison of the both simulation model and the actual positioning system are presented for various path tracking velocities. Resultant root mean square (rms) errors of the before and after controller parameter tuning studies are presented for various velocites both in micrometers and percentages. Finally, before and after results of a nonlinear trajectory tracking improvement experiment is presented with figures.

## 5.1 Spot Size and Power Experiments

As mentioned in chapter 2, optical lens of the laser system is changed and a 56 mm diameter lens is implemented to the laser system instead of a 160 mm diameter original one. This implementation induced several changes on the system properties like intensity, focal length and spot size. Focal length of the laser system is decreased as expected from 263 mm to 153 mm. To observe the influences of modification of optical lens of the laser system on other laser parameters like spot size and power some experiments are performed. These experiments are carried out with variable power, fixed frequency and velocity parameters.

The aim of decreasing spot size is about performing smaller dimension with the enhanced laser micromachining system. Change of optical lens, decreases output beam diameter and the lower beam diameter increases the intensity of the beam. In order to observe this, experiments are started by low powers and it is clearly stated by some authors [25, 26, 27] that lower intensities decrease spot size, which meets with the purpose of this study.

Spot size results became observable with % 1 power and experiments are resumed until % 9 power. Chart on Figure 5.1 is created to represent the results of these experiments.

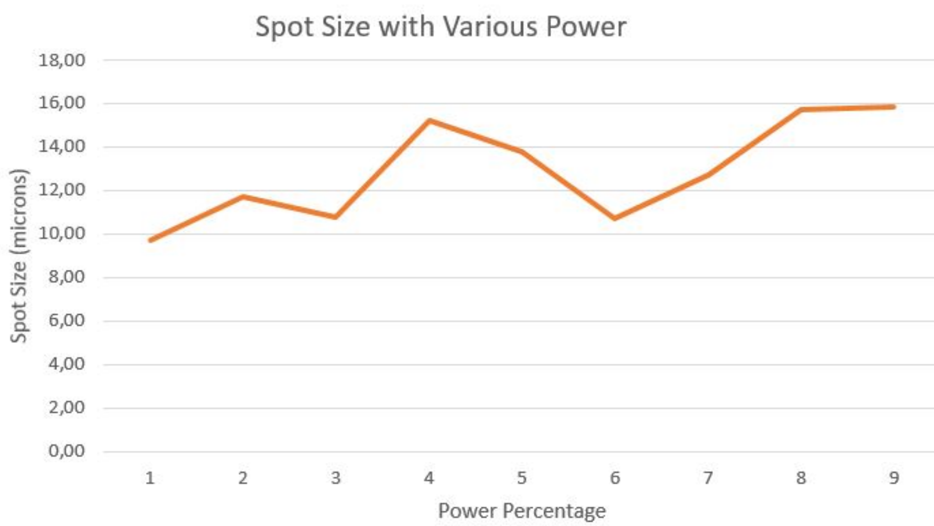


Figure 5.1: Spot Size vs Power Percentage

At the end of the experiments, it obvious that spot size of the system is decreased down to 10 microns where the power is increased which is dependent on intensity.

## 5.2 SimMechanics and Simulations

### 5.2.1 Developing Simulation Model and Optimizations

For simulation studies, a solid model of the manipulator is established in SolidWorks and imported to SimMechanics to obtain a dynamic model. The dynamic model is created by using the original structural properties and kinematic models of the positioning system. However, the whole system cannot be modeled because of some unknown specifications of the manipulator. These unknown properties are mass and actuator properties of the positioning system. In order to implement these unmodeled components, some optimizations are performed to get an approximate dynamic model of the actual positioning system.

Table 5.1: Weights of Parts in SimMechanics Model

| Moving Platform | L Part 1 | L Part 2 | Moving Base 1 | Moving Base 2 |
|---|---|---|---|---|
| 0.25 kg | 0.1 kg | 0.1 kg | 1 kg | 1 kg |

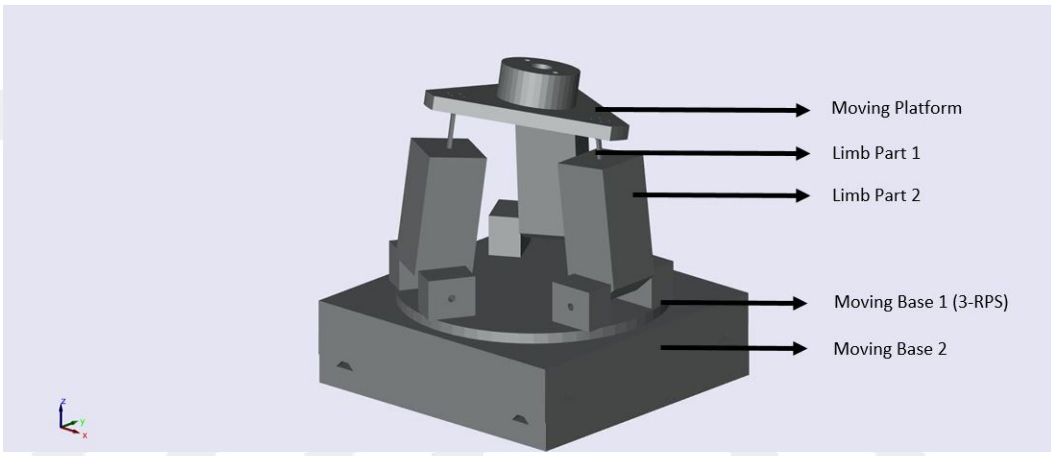


Figure 5.2: Mass Properties of the Simulation Model

First optimization is done by adapting mass properties of the actual positioning system to SimMechanics model. Adapted masses are listed in Table 5.1, notice that these are not real masses. By the help of gravity compensation of positioning system, dynamic model is optimized by using small masses. Gravity compensation system releases masses of the components of the positioning system and creates minimal air pressure forces on the actuators of the manipulator. Given masses correspond to with the components of the simulation model in Figure 5.2.

Second optimization is performed for unmodeled actuators of the manipulator model. To get a better performance from the dynamics model, these parts are also added to the simulation model. This is done by inserting amplifying coefficients to the simulation model as gains on each actuator. These coefficients are placed to be a value of 50 between PID controllers and SimMechanics model of the positioning system. These amplifiers are tuned by considering the measured positioning system. Resultant gain is found after the optimizations. Figure 5.3 illustrates amplifier coefficients on the simulation model.

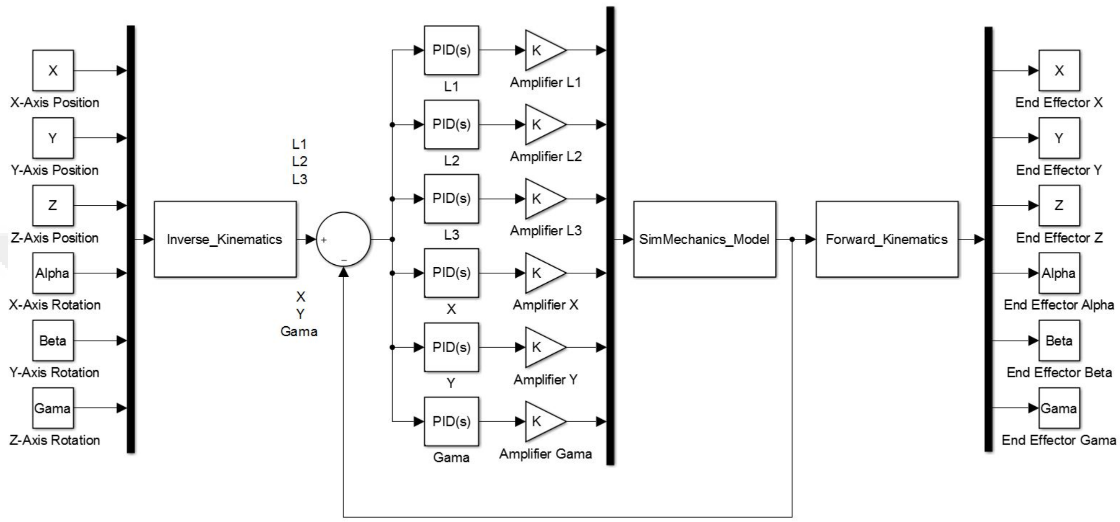


Figure 5.3: Representative Schema for Simulation System

After optimizations, a convenient dynamic model is created to be used for simulations. Simulation schema is presented in Figure 5.3.

## 5.3 Trajectory Tracking Performance Investigations

While performing trajectory tracking performance investigations for the positioning system, errors of the actuators on the active joints are taken into account for given trajectory. Calculating the performance error of the laser micromachining process can be performed in different ways. A way of calculating this error is to measure the features of the manufactured workpiece. For 2D laser micromachining, this can be done with measuring the engraved parts of the manufactured material by using microscopes. In 3D case, performing measurements with microscope on the manufactured 3D parts is not always a reliable way because of the surface properties of the materials. For this case some other techniques are being used. One of them is using coordinate measuring machine (CMM). They can measure with a 0.1 micrometer uncertainty for coordinate measurement applications [28].

In this study, the laser system is fixed and does not perform any positioning. Positioning error of the manipulation system can be observed by comparing measured positioning informations from encoders of the actuators. It is an easy, fast and reliable way for our machining experiments. This is the way that we used in our performance improvement studies. The results given in the following sections are obtained with this method.

### 5.3.1 Nonlinear Trajectory Tracking Simulations

Initial control system improvement studies are started with testing the performance of the positioning system with a desired nonlinear trajectory. This trajectory is given in Figure 5.4 with a blue line. In Figure 5.4, measured nonlinear trajectory tracking performance of the positioning system is presented with a green line.

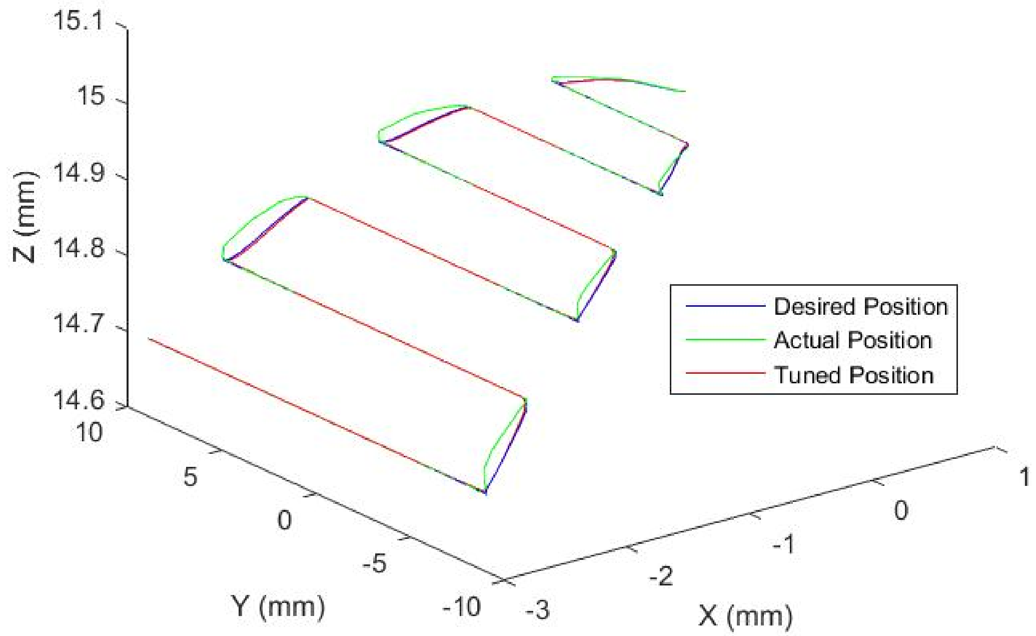


Figure 5.4: Tuned Trajectory Comparison with Desired and Measured Results (Simulation)

For simulations, generated nonlinear trajectory is imported to the simulation model and the response of all the active joints are examined. Simulation strategy is given in Figure 5.3. As presented in Figure 5.3, desired position information of the trajectory is imported to inverse kinematics of the positioning system. After inverse kinematics, desired joint space informations are gathered. Then, desired joint space informations are sent to the controllers and SimMechanics model of the positioning system. The measured joint space informations which are obtained from the SimMechanics model and they are compared with the desired joint space informations of the nonlinear trajectory. Finally, error of the joint space positioning informations are minimized with PID controllers of the joint actuators.

For tuning PID control parameters of the PID controllers on joint actuators, manual tuning technique is used. Initially, integral and derivative gains are set to zero. Proportional gains are increased until observing the oscillations with a response that is close to the setpoint. Then half of the proportinal gains are used and integral and derivative gains are increased incrementally upto obtaining a good tracking performance. This procedure is applied for all link actuators.

Figure 5.5 to Figure 5.13 show the position error informations of each link in simulations. Measured and simulation error of joint actuators are given for link 1(L1), link 2(L2) and link 3(L3) with three different tracking velocities. Rms errors of tracking simulations are presented in Table 5.2, Table 5.3 and Table 5.4 for each link and velocities. These nonlinear trajectory tracking performances are transformed from joint actuator position informations by forward kinematics of the positioning system.

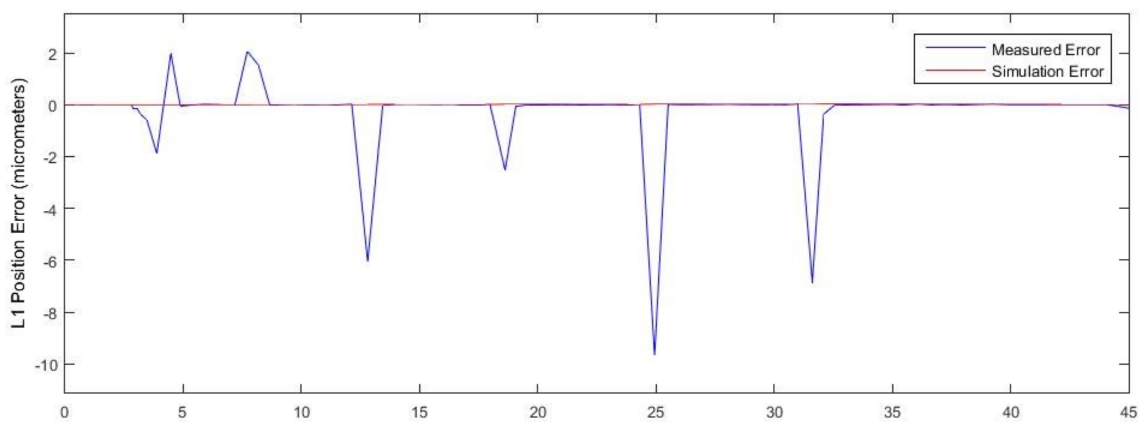


Figure 5.5: Measured and Tuned Positions of Link 1 for Nonlinear Trajectory Tracking (Simulation) with a 5 mm/sec Velocity

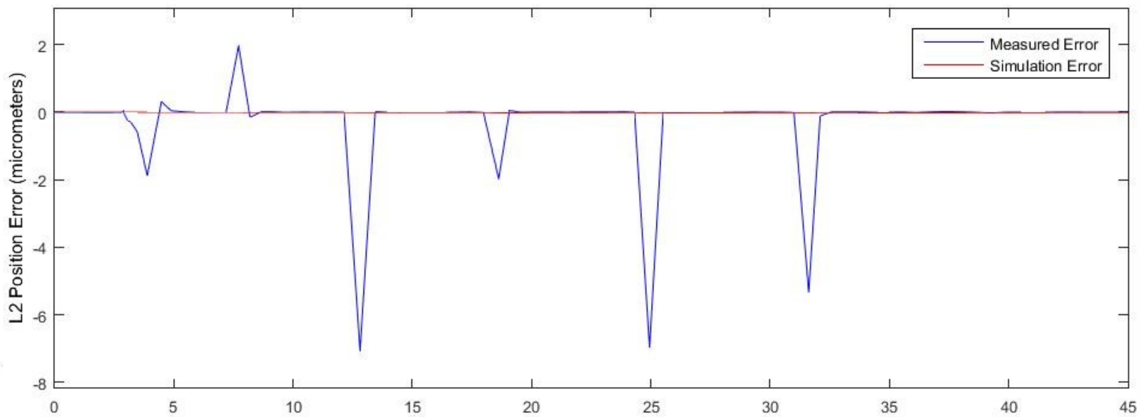


Figure 5.6: Measured and Tuned Positions of Link 2 for Nonlinear Trajectory Tracking (Simulation) with a 5 mm/sec Velocity

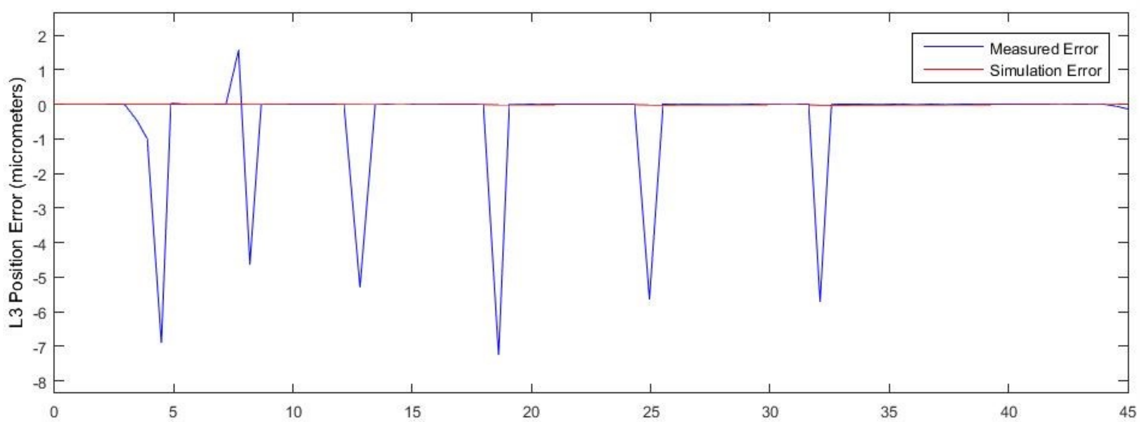


Figure 5.7: Measured and Tuned Positions of Link 3 for Nonlinear Trajectory Tracking (Simulation) with a 5 mm/sec Velocity

Table 5.2: Root Mean Square of Position Errors for Link Actuators (Velocity: 5 mm/sec)

| | Measured Error(micrometer) | Simulation Error(micrometer) |
|---|---|---|
| L1 | 2.57 | 0.0123 |
| L2 | 1.71 | 0.0123 |
| L3 | 1.43 | 0.0123 |

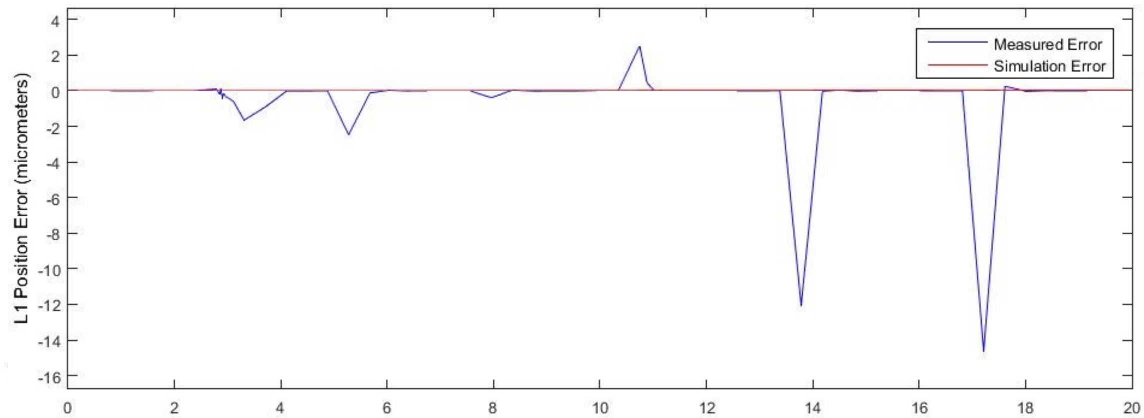


Figure 5.8: Measured and Tuned Positions of Link 1 for Nonlinear Trajectory Tracking (Simulation) with a 10 mm/sec Velocity

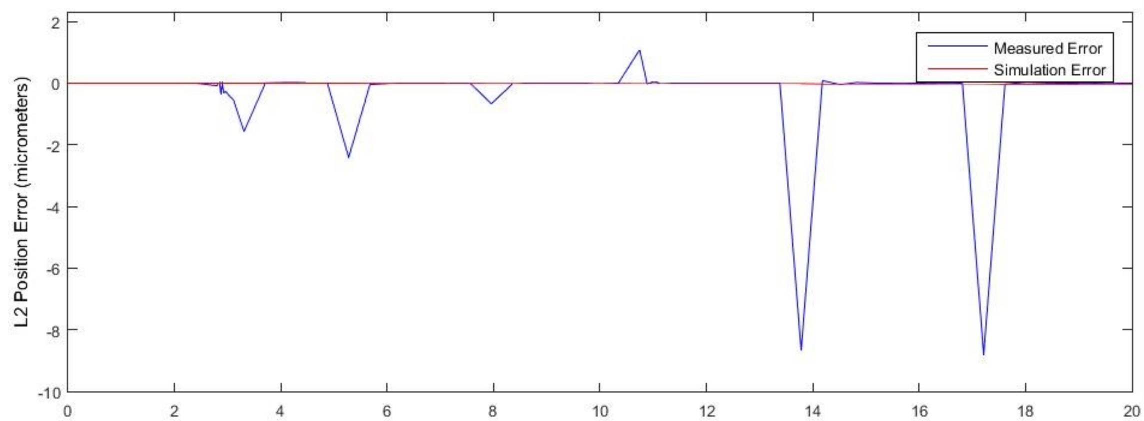


Figure 5.9: Measured and Tuned Positions of Link 2 for Nonlinear Trajectory Tracking (Simulation) with a 10 mm/sec Velocity

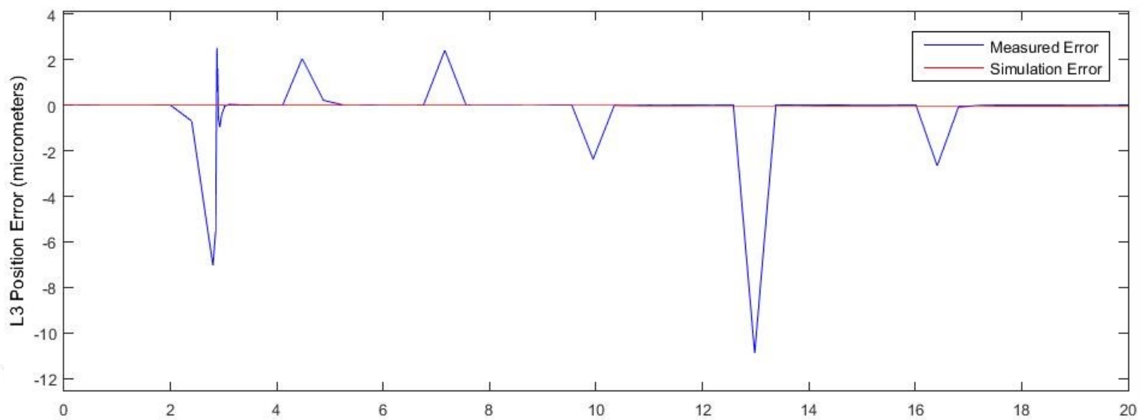


Figure 5.10: Measured and Tuned Positions of Link 3 for Nonlinear Trajectory Tracking (Simulation) with a 10 mm/sec Velocity

Table 5.3: Root Mean Square of Position Errors for Link Actuators (Velocity: 10 mm/sec)

| | Measured Error(micrometer) | Simulation Error(micrometer) |
|---|---|---|
| L1 | 3.04 | 0.016 |
| L2 | 1.78 | 0.016 |
| L3 | 1.83 | 0.016 |

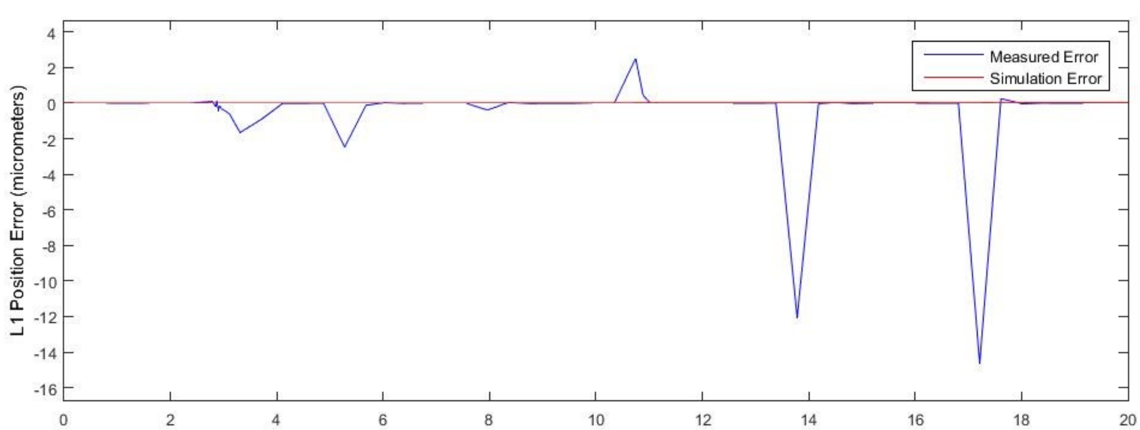


Figure 5.11: Measured and Tuned Positions of Link 1 for Nonlinear Trajectory Tracking (Simulation) with a 15 mm/sec Velocity

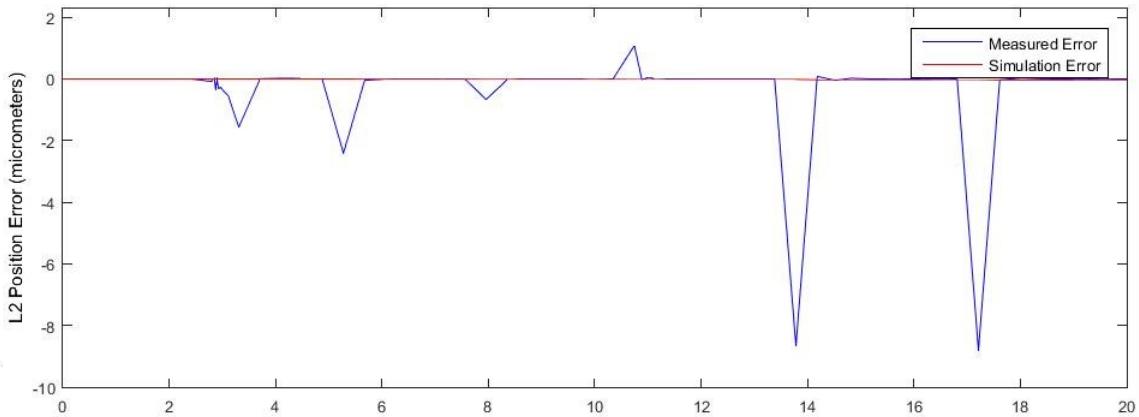


Figure 5.12: Measured and Tuned Positions of Link 2 for Nonlinear Trajectory Tracking (Simulation) with a 15 mm/sec Velocity

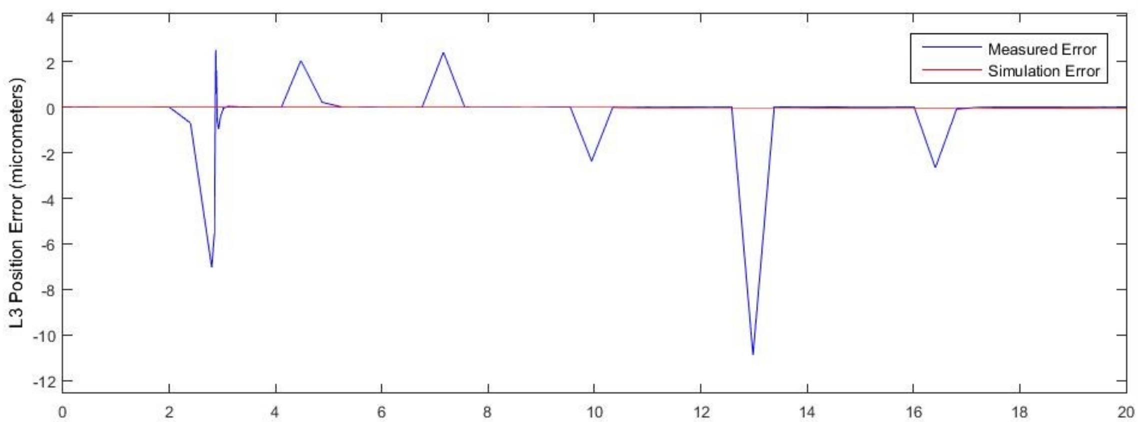


Figure 5.13: Measured and Tuned Positions of Link 3 for Nonlinear Trajectory Tracking (Simulation) with a 15 mm/sec Velocity

Table 5.4: Root Mean Square of Position Errors for Link Actuators (Velocity: 15 mm/sec)

| | Measured Error(micrometer) | Simulation Error(micrometer) |
|---|---|---|
| L1 | 4.15 | 0.0229 |
| L2 | 2 | 0.0229 |
| L3 | 2.36 | 0.0229 |

The presented results in Figure 5.5 - Figure 5.13 are obtained by using PID parameters which are listed in Table 5.5. These parameters are used in PID controllers of limb actuators in simulation. Results of the simulations show that nonlinear trajectory tracking performance can be improved by tuning PID control parameters of the manipulations system. Rms error of the link actuators and nonlinear trajectory tracking performance of the simulations are presented inTable 5.2, Table 5.3 and Table 5.4.

Table 5.5: PID Parameters (Simulation)

| Proportional Gain | Integral Gain | Derivative Gain |
|---|---|---|
| 10 | 0.1 | 0.07 |

As can be observed from Figure 5.5 to Figure 5.13, trajectory tracking errors of link actuators are decreased for all cases. PID control parameters which are obtained from the simulations are used in the positioning system.

### 5.3.2 Nonlinear Trajectory Tracking Experiments (Manipulator)

In simulations, gains of PID controllers are tuned to improve the performance of the positioning system for given nonlinear trajectory. Results of the simulation show that, performance of the system can be improved by tuning PID controller parameters. Simulation results gave us an opinion about the PID controller parameters which we need to import to the positioning system.

Software of the manipulator system provides measured motor position plots for all actuated joints during a trajectory tracking performance from the encoders of the actuators. By the help of modeled kinematic of the positioning system, measured and desired motor position plots can be converted to end effector position informations. By comparing results of measured desired informations, error of the positioning system can be calculated for both cartesian and joint space performance of the manipulator.

Results presented from Figure 5.14 to 5.23 show the comparison of experimental results of actual manipulator for the given nonlinear trajectory. In Figure 5.23, desired, measured and tuned nonlinear trajectory tracking performances of the positioning system are presented. From Figure 5.14 to 5.22, trajectory tracking performances of measured and tuned experimental results compared for actuators on the links of the positioning system.

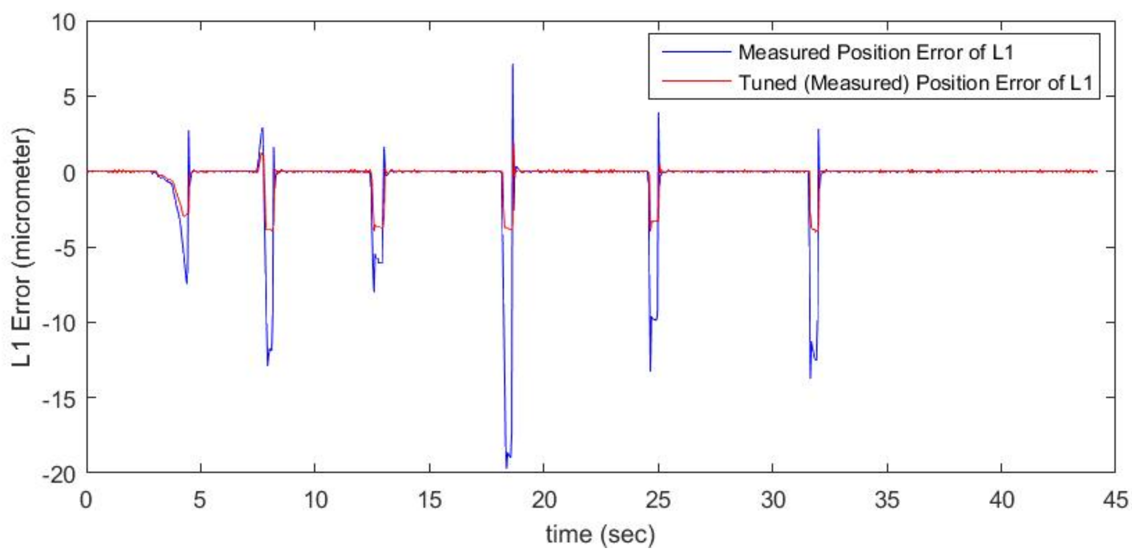


Figure 5.14: Measured and Tuned (Measured) Positions of Link 1 for Nonlinear Trajectory Tracking (Manipulator) with a 5 mm/sec Velocity

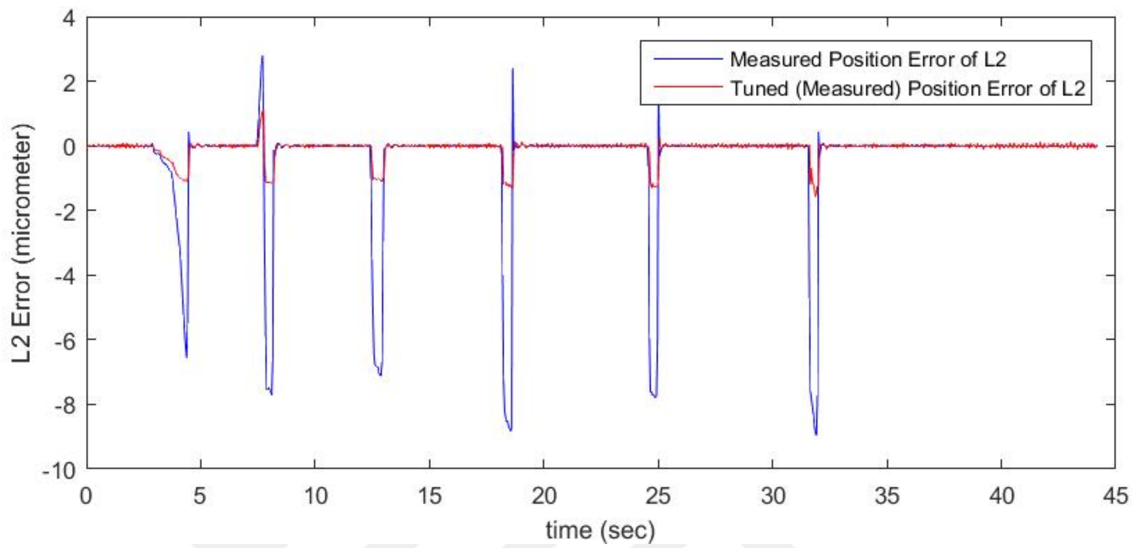


Figure 5.15: Measured and Tuned (Measured) Positions of Link 2 for Nonlinear Trajectory Tracking (Manipulator) with a 5 mm/sec Velocity

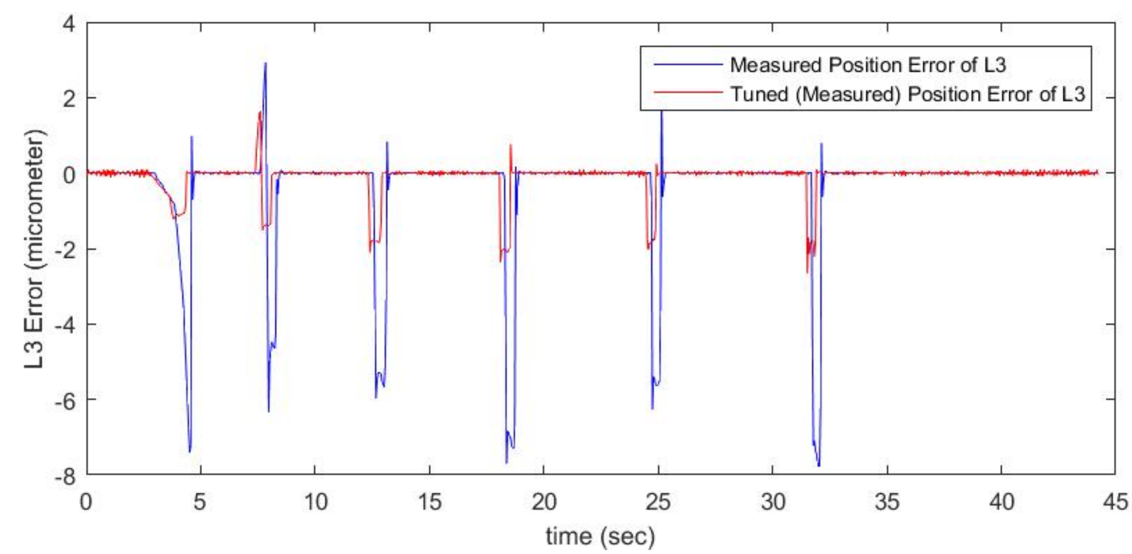


Figure 5.16: Measured and Tuned (Measured) Positions of Link 3 for Nonlinear Trajectory Tracking (Manipulator) with a 5 mm/sec Velocity

Table 5.6: Root Mean Square of Position Errors for Link Actuators (Velocity: 5 mm/sec)

| | Measured Error(micrometer) | Tuned Error(micrometer) |
|---|---|---|
| L1 | 2.57 | 0.86 |
| L2 | 1.71 | 0.3 |
| L3 | 1.44 | 0.44 |

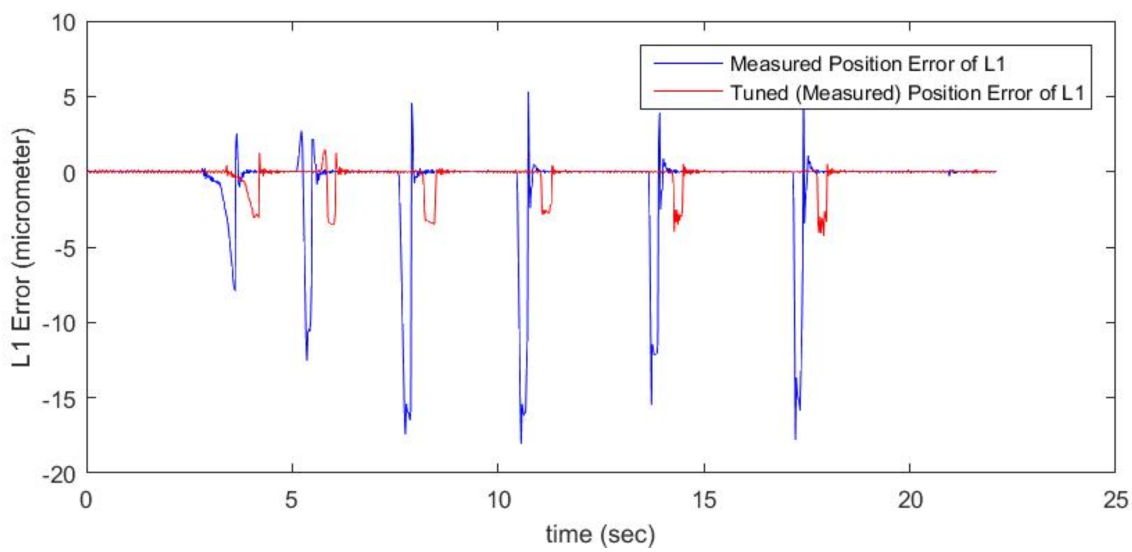


Figure 5.17: Measured and Tuned (Measured) Positions of Link 1 for Nonlinear Trajectory Tracking (Manipulator) with a 10 mm/sec Velocity

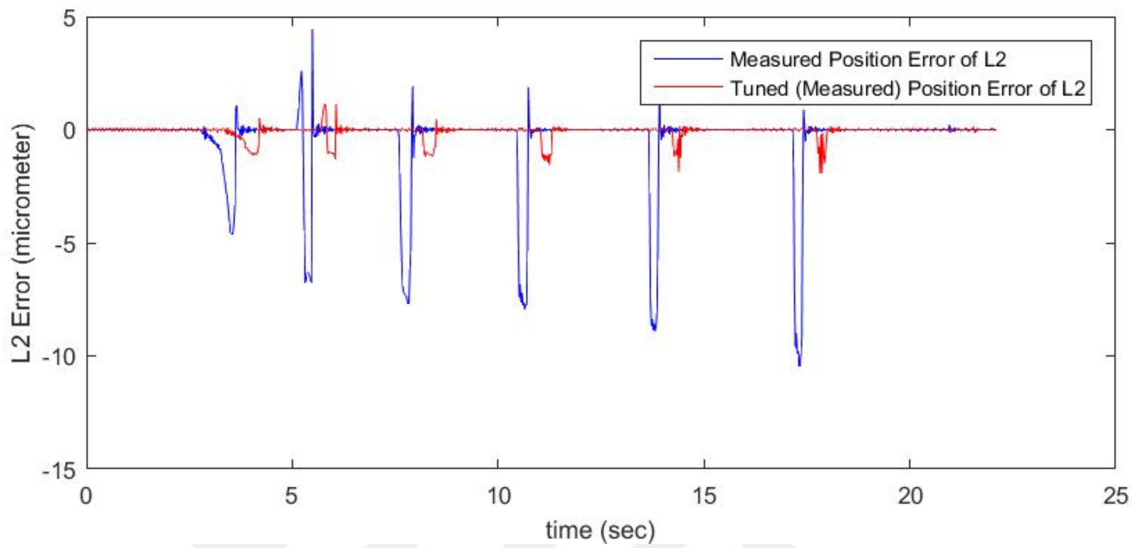


Figure 5.18: Measured and Tuned (Measured) Positions of Link 2 for Nonlinear Trajectory Tracking (Manipulator) with a 10 mm/sec Velocity

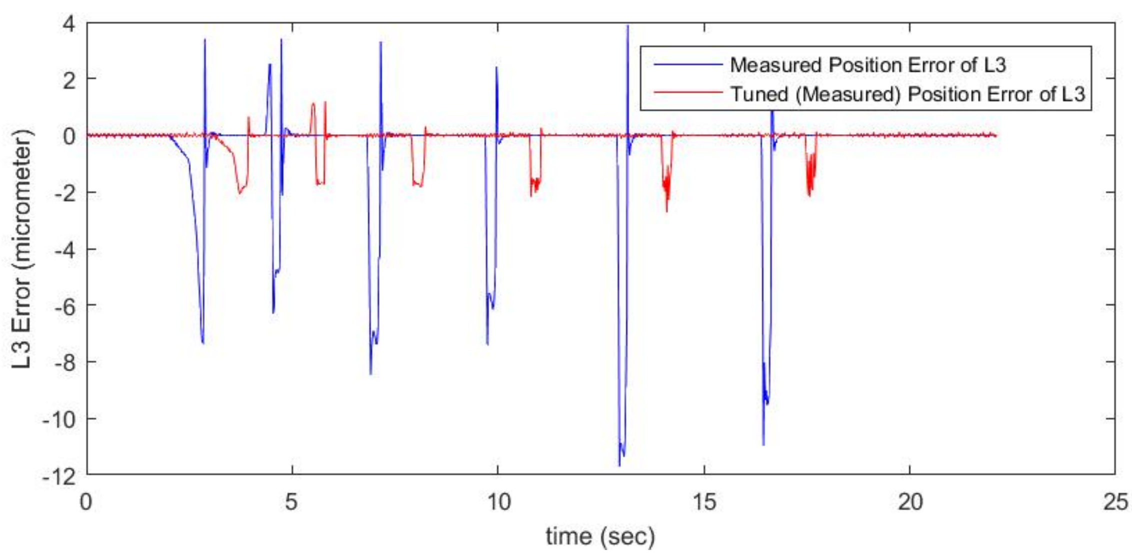


Figure 5.19: Measured and Tuned (Measured) Positions of Link 3 for Nonlinear Trajectory Tracking (Manipulator) with a 10 mm/sec Velocity

Table 5.7: Root Mean Square of Position Errors for Link Actuators (Velocity: 10 mm/sec)

| | Measured Error(micrometer) | Tuned Error(micrometer) |
|---|---|---|
| L1 | 3.04 | 0.79 |
| L2 | 1.78 | 0.3 |
| L3 | 1.83 | 0.46 |

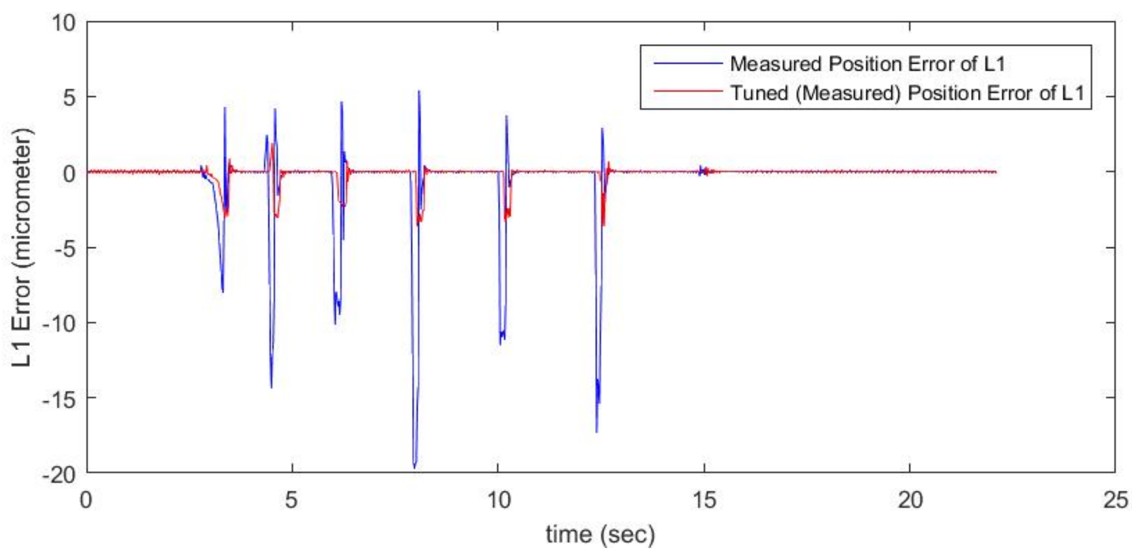


Figure 5.20: Measured and Tuned (Measured) Positions of Link 1 for Nonlinear Trajectory Tracking (Manipulator) with a 15 mm/sec Velocity

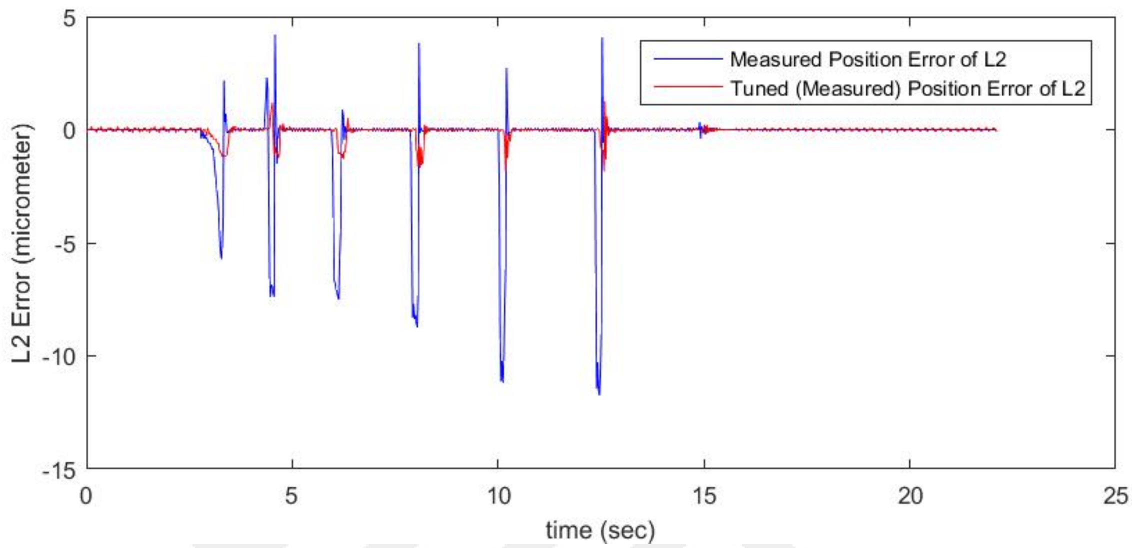


Figure 5.21: Measured and Tuned (Measured) Positions of Link 2 for Nonlinear Trajectory Tracking (Manipulator) with a 15 mm/sec Velocity

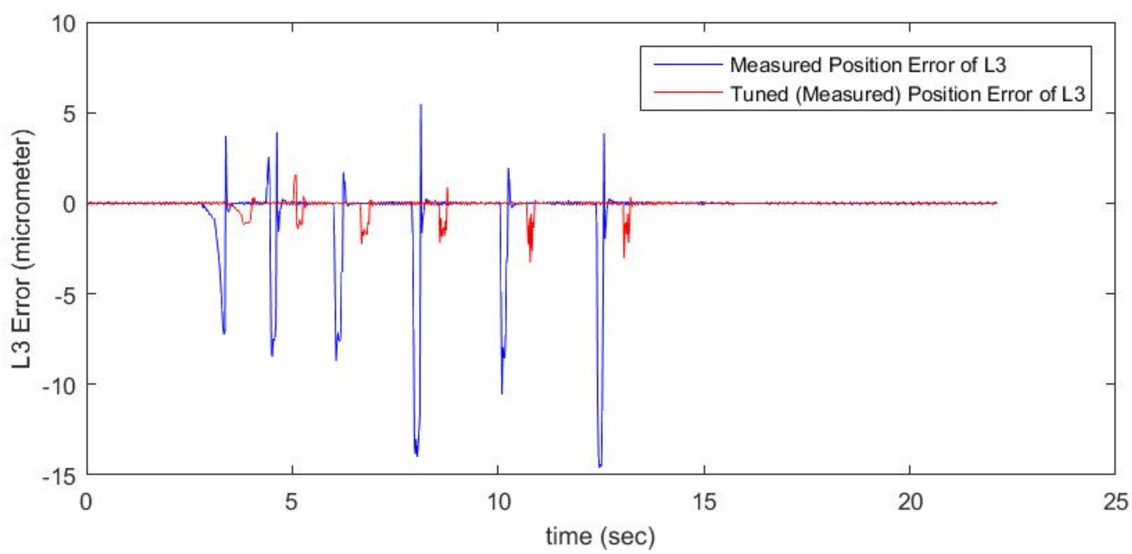


Figure 5.22: Measured and Tuned (Measured) Positions of Link 3 for Nonlinear Trajectory Tracking (Manipulator) with a 15 mm/sec Velocity

Table 5.8: Root Mean Square of Position Errors for Link Actuators (Velocity: 15 mm/sec)

| | Measured Error(micrometer) | Tuned Error(micrometer) |
|---|---|---|
| L1 | 4.15 | 0.58 |
| L2 | 2 | 0.26 |
| L3 | 2.36 | 0.35 |

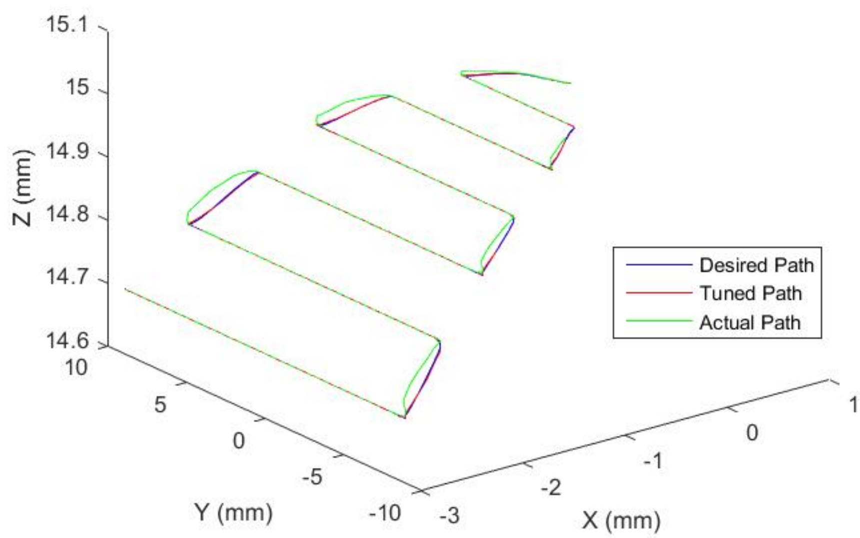


Figure 5.23: Tuned Trajectory Comparison with Measured Trajectory Tracking Results (Manipulator)

Presented results in Figure 5.14 to 5.23 are obtained by using PID parameters listed in Table 5.9. These parameters are used in PID controllers of the link actuators of the positioning system. From the figures, we can say that, by tuning PID control parameters the performance of the positioning system is improved and a better nonlinear trajectory tracking performance is obtained.

For PID control parameter tuning studies of the positioning system, manual tuning techniques are used as explained in simulations. Proportional gains of the PID controllers of the link actuator are initally set to 10 which is obtained in simulation studies. As stated in [23], integral and derivative gains are implemented as zero. Positioning system is started to oscillate and failed with these gains and by considering the mentioned tuning technique, new proportional gains of the link actuators are set to 1. Again, manipulator is started to oscillate but did not fail this time. Then, proportional gains of the link actuators are set to 0.5. With a 0.5 proportional gain the manipulator stoped oscillation and started to work smoothly. After that, integral and derivative gains are increased with small increments. Finally, the best results are obtained with the parameters which are presented in Table 5.9. Initial PID control parameters of the positioning system are also given in Table 5.9.

Table 5.9: PID Parameters (Manipulator)

| | Proportional Gain | Integral Gain | Derivative Gain |
|---|---|---|---|
| After Tuning | 0.5 | 0.1 | 0.07 |
| Before Tuning | 0.1 | 0.1 | 0.5 |

Rms error of link actuators are presented in Table 5.6 to Table 5.8 for 5 mm/sec, 10 mm/sec and 15 mm/sec velocities. From the results, we can say that the performance of the positioning system is improved for the given nonlinear trajectory. In Table 5.10 all results obtained from simulations and expeeriments are presented both in micrometers and percentages. Nonlinear trajectory tracking error of the positioning system for 5 mm/sec tracking velocity is decreased about %72.33 (1.37 micrometer). For 10 mm/sec tracking velocity, tracking error is decreased about %77.33 (1.71 micrometer) and for 15 mm/sec tracking velocity, tracking error is decreased about %86 (2.44 micrometer) with manually tuned PID control parameters. In simulations, nonlinear trajectory tracking error of the simulation model is decreased around %99(1.89, 2.2 and 2.81 micrometers respectively) for all tracking velocities.

Table 5.10: Root Mean Square of Position Errors for Trajectory Tracking and Link Actuators with Microns and Percentages

| | Measured Error | Tuned Error | Simulation Error |
|---|---|---|---|
| L1 (5 mm/sec) | 2.57 | 0.86 (%66) | 0.0123 (%99) |
| L2 (5 mm/sec) | 1.71 | 0.3 (%82) | 0.0123 (%99) |
| L3 (5 mm/sec) | 1.44 | 0.44 (%69) | 0.0123 (%99) |
| L1 (10 mm/sec) | 3.04 | 0.79 (%74) | 0.016 (%99) |
| L2 (10 mm/sec) | 1.78 | 0.3 (%83) | 0.016 (%99) |
| L3 (10 mm/sec) | 1.84 | 0.45 (%75) | 0.016(%99) |
| L1 (15 mm/sec) | 4.15 | 0.58 (%86) | 0.0229 (%99) |
| L2 (15 mm/sec) | 2 | 0.26 (%87) | 0.0229 (%99) |
| L3 (15 mm/sec) | 2.36 | 0.35 (%85) | 0.0229 (%99) |

Results which are presented in Table 5.10 show that the trajectory tracking of the positioning system is decreased submicron level. This valid for all velocities and actuators by using presented controller parameters in Table 5.9.

## 5.4 Laser Micromachining on Nonlinear Trajectory

In order to observe the improvements of the overall laser micromachining system on nonlinear contoured surfaces, an experiment is performed. Desired nonlinear trajectory is uploaded to the positioning system and the performance of the laser micromachining system on a cylindrical surface is tested. Figure 5.24 shows the result of performed experiment. Table 5.11 presents the tracking error of the actuators and projection of the error.

Table 5.11: Root Mean Square of Position Errors for Trajectory Tracking

| | Measured Error | Tuned Error |
|---|---|---|
| L1 | 4.15 | 0.58 |
| L2 | 2 | 0.26 |
| L3 | 2.36 | 0.35 |
| X | 1.3 | 0.24 |
| Y | 1.8 | 0.35 |
| Z | 1.84 | 0.55 |

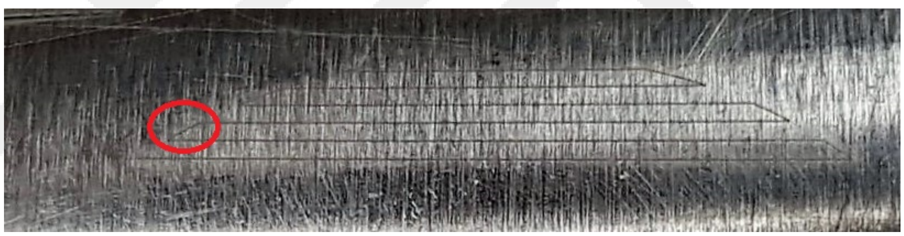

Figure 5.24: Laser Micromachining Experiment on Cylindrical Surface

Spot size of the laser is measured as 20 micrometers during the process and velocity of the tracking was 15 mm/sec . The overall error of the manipulator is decreased 1.5-4.5 to 0.3-0.9 micrometers. With a 20 micrometer spot size, it is really difficult to observe the performance improvement of micromachining for given errors in three cartesian axes. In Figure 5.25 and Figure 5.26, a corner of the manufactured pattern is given to compare the measured and tuned nonlinear trajectory tracking results. This is the most clear result among the other corners for observing the improvement and it is circuled in Figure 5.24.

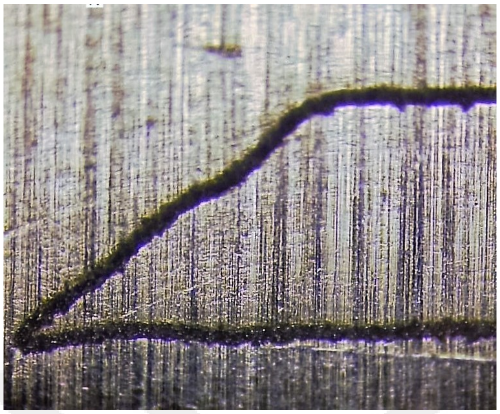

Figure 5.25: Laser Micromachining Result with Initial PID Parameters

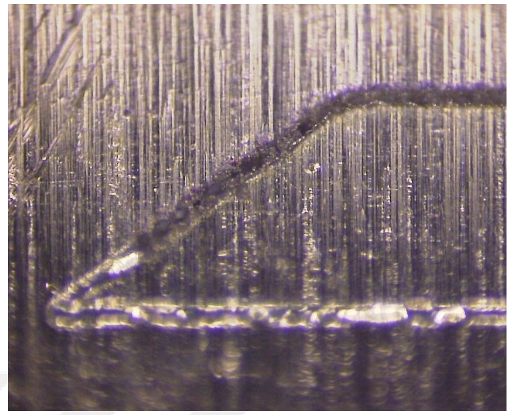

Figure 5.26: Laser Micromachining Result with Tuned PID Parameters

To sum up, spot size improvements and development and optimization of simulation model of the positioning system is explained and presented. Nonlinear trajectory tracking performance comparison of the both simulation model and the positioning system are presented. Resultant root mean square(rms) errors of the before and after controller parameter tuning studies are presented in percentages for both joint space and cartesian space informations. Finally, before and after results of a nonlinear trajectory tracking improvement experiment is presented with figures. According to these results, performance of the overall system on nonlinaer contoured surfaces is improved. If we consider the current results that we obtained with introduced nonlinear trajectory, rms error is decreased about %75 - 80. Spot size of the laser system was 20 micrometers during the experiments and that influenced the results of the experiments. However, improvements can be observed clearly.

# Chapter 6

# Conclusions

The aim of this study was to develop a multi-axis laser micro machining system which is suitable for machining on nonlinear contoured surfaces. In the scope of this purpose, a laser micromachining system is established with selected components. After establishing the system, several calibration and validation studies are performed. After that, various improvements are implemented on the laser micromachining system for performance enhancements.

Established laser micromachining system is tested to investigate initial characteristics of individual components. During these investigations, validation and calibration tests are performed. Validation and calibration studies are completed in several steps. The first step is to get both laser system and positioning system work with the same coordinate system. They need to work in same coordinate system to perform machining with a zero offset, otherwise manufactured parts would have a constant error. In this work, this is done by perfectly assembling the individual systems on mentioned vibration absorber table. Some experiments are also performed to see the coincidence of coordinate systems. Then, optical lens of the laser system is changed with a desired one to decrease the spot size during manufacturing process. To obtain desired spot size, various experiments are performed and they are presented in chapter 5. The spot size decreased downto 10 microns from at least 70 microns. During performing spot size investigations, power properties of the laser system is also tested. As mentioned in chapter 5, changing optical lens of the laser system effects both spot size and intensity of the laser beam. After the update of the optical lens, the smallest spot sizes can be obtained with a power range from 1 percent to 9 percent. Also, the contoller of the laser system is decomposed and an M series NI-SCB 68 DAQ system integrated to laser machine. After this integration, the laser system is became capable of changing its power during a manufacturing process. For this improvement a new user interface is designed in Labview software to use the laser system independent from its own interface and controller.

After completing improvements on the laser system and performing validation - calibration tests on the laser micromachining system, next step is to investigate positioning system. For this purpose, kinematic and dynamic models of the positioning system are created. Dynamic model is created on SimMechanics software by using geometrical properties of the real positioning system and some optimization studies are performed as discussed in chapter 4. During these studies a nonlinear trajectory is created to check the performace of the positioning system in nonlinear case. As discussed in previous chapters, trajectory tracking results of the positioning system were not good enough to get a satisfying resultant trajectory. To overcome this issue, PID controllers are integrated to active joints of the dynamic model of the positioning system and PID control parameters are tuned by manually tuning technique. Then, obtained PID control parameters are used in the actual positioning system. Result of this integration was not good enough and the positioning system was oscillating. To obtain desired parameters, PID control parameter tuning studies are also performed on the real positioning system by using manually tuning technique. PID control parameters obtained for the real and simulation model of the manipulator presented in chapter 5. Integral and derivative gains of both simulations and measured positioning system are same but proportional gains are different. Probably, this difference is because of unmodeled dynamics of the positioning system. At the end, a nonlinear pattern is textured on a cylindrical contoured surface.

As can be concluded from the results of the experiments and simulations, nonlinear trajectory tracking error of the positioning system is minimized. Spot size is decreased down to 10 micros and the laser micromachining system characteristics are enhanced to perform micron level patterns on nonlinear contoured surfaces. Results of the performed fabrication show that, nonlinear surface texturing performance of the laser micromachining system is improved. However, spot size of the laser system must be decreased more to observe the improvements more clearly. The laser micromachining system that we developed is capable of performing with various laser power during fabrication process. With this capability, it seems possible to create 3D patterns on planar workpieces. This issue can be a consideration for following research studies with this laser micromachining system.

# Bibliography


[1] M. Gower, "Industrial applications of laser micro-machining," *Optics Express*, vol. 7, no. 2, pp. 56–67, 2000.

[2] A. G. J.P.H. Burt and J. T. C.J. Hayden, "Laser micromachining of biofactory-on-a-chip devices," *Proc. SPIE*, vol. 4637, pp. 305–317, 2002.

[3] I. S.-B. ForK.L. Boehlen, "Laser micromachining of high-density optical structures on large substrates," *Proc. SPIE*, vol. 5339, pp. 118–126, 2004.

[4] A. S. Holmes, J. E. Pedder, and K. L. Boehlen, "Advanced laser micromachining processes for mems and optical applications," *Proc. SPIE*, vol. 6261, 2006.

[5] I. S. K. Edin Golubovic, E. A. B. Ahmet O. Nergiz, and A. Sabanovic, "Design and control of laser micromachining workstation," *IEEE International Workshop on Advanced Motion Control*, vol. 12, 2012.

[6] D. B. Pavel Penchev, S. Dimov, and S. L. Soo, "Novel manufacturing platform for scale up production of miniaturized parts," *INTERNATIONAL WORKSHOP ON MICROFACTORIES*, pp. 231 – 238, 2014.

[7] AEROTECH, "Capabilities in laser processing and micromachining," Aug. 2016.

[8] B. P. Ali Gkhan Demir and C. A. Biffi, "Fibre laser cutting and chemical etching of az31 for manufacturing biodegradable stents," *Hindawi Publishing Corporation Advances in Materials Science and Engineering*, vol. 2013, 2013.

[9] Q. Xia and S. Y. Chou, “Applications of excimer laser in nanofabrication,” *Applied Physics*, vol. 98, pp. 9–59, 2010.

[10] A. Y. Y. L. Li, “Development of a 3d artificial compound eye,” *Optics Express*, vol. 18, pp. 18125–18137, 2010.

[11] L. Li and A. Y. Yi, “Microfabrication on a curved surface using 3d microlens array projection,” *Journal of Micromechanics and Microengineering*, vol. 19, 2009.

[12] ALPhANOV, “Development and design of custom laser micromachining systems,” Aug. 2016.

[13] R. R. H. Pantsar and A. J. P. Laakso, “Advances in 3d laser processing in mold technology,” *25th International Congress on Applications of Lasers and Electro Optics*, 2006.

[14] F. LTD, “Laser surface texturing,” Aug. 2016.

[15] J. B. NC, “Robot arm laser cutting machine,” Aug. 2016.

[16] F. K. Andreas Ostendorf, U. K. Guenther Kamlage, J. S. Juergen Koch, T. B. Niko Baersh, and B. N. Chichkov, “3d laser microfabrication: Principles and applications,” in *3D Laser Microfabrication* (H. M. andSaulius Juodkazis, ed.), ch. 12, pp. 341–377, Wiley-VCH Verlag GmbH and Co KGaA, Weinheim, 2006.

[17] M. L. A. Cinthya Toro Salazar and C. A. Rinaldi, “Nanostructuring of material surfaces by laser ablation,” *InTech*, vol. 10.5772/62638, 2016.

[18] M. PHOTONICS, “Mfp q-switched pulsed fiber laser,” Aug. 2016.

[19] A. INDUSTRIES, “Parallel linematics motion system,” Aug. 2016.

[20] A. INDUSTRIES, “Parallel linematics motion system - specifications,” Aug. 2016.

[21] I. T. Committee, “The ilda standard projector,” *INTERNATIONAL LASER DISPLAY ASSOCIATION*, 1999.

[22] J. Diebel, "Representing attitude: Euler angles, unit quaternions, and rotation vectors," 2006.

[23] K. Ogata, "Modern control engineering," in *Modern Control Engineering* (M. J. Horton, ed.), Pearson Education International, 2002.

[24] N. Instruments, "Fundamentals of mation control," Aug. 2016.

[25] G. JACOBS, "Understanding spot size for laser scanning," *PROFESSIONAL SURVEYOR MAGAZINE*, 2006.

[26] N. Corporation, "Gaussian beam optics," Aug. 2016.

[27] H. Wang and T. Chong, "Spot size and depth of focus in optical data storage system," *Optical Engineering*, vol. 46, no. 6, 2007.

[28] F. M. A. Kng and R. Thalmann, "Ultraprecision micro-cmm using a low force 3d touch probe," *Measurement Science and Technology 18*, pp. 319–327, 2007.

# Appendix A

# Code

## A.1 Forward Kinematics

### forwardkinematicsmain.m

```
L1 = m1/819200;                    %L1 motor position(limb)
L2 = m2/819200;                    %L2 motor position(limb)
L3 = m3/819200;                    %L3 motor position(limb)
L4 = (m4/819200);                  %L4 motor position X-dir
L5 = (m5/819200);                  %L5 motor position Y-dir
L6 =  (m6/716526.93333);      %L6 motor position Z-dir

for i = 1:length(L1)
[C0(i),C1(i),C2(i),C6(i),C7(i),C8(i)] =
 frwdmodular(L1(i),L2(i),L3(i),L4(i),L5(i),L6(i));
end
```

### frwdmodular.m

```
function [C0,C1,C2,C6,C7,C8] = frwdmodular(L1,L2,L3,L4,L5,L6)
```

```
%GUESSED VALUES THOSE WILL BE MODIFIED


KinPosAxisB=15; % Guessed rotation
KinPosAxisA=15; % Guessed rotation
C8=15; % Guessed Z—axis position

% SCALE FACTORS FOR CONVERTING MOTOR UNITS TO MM
Q1=1; %FOR AXIS 1
Q2=1 ; %FOR AXIS 2
Q3=1 ; %FOR AXIS 3
Q4=1; %FOR AXIS 4
Q5=1 ; %FOR AXIS 5
Q6=1; %FOR AXIS 6

% MECHANICAL COORD VALUES
Zmax=277.409215;     %Maximum Z Axis Position
Zmin=218.630447;     %Minimum Z Axis Position
Lmax=280.35;         %Maximum Limb Length
Lmin=222.35;         %Minimum Limb Length
dB=153;          %Bottom Plate Diameter
dC=112.5;            %Top Plate Diameter


% DEFAULT END EFFECTOR OFFSETS
O1=0;
O2=0;
O3=0;
O4=0;
O5=0;
O6=61;

% FORWARD KINEMATIC CONVERGENCE RATIOS
Q6023=5;
Q6033=5;
Q6093=1.2;
Q6201=50;

%Forward Kinematics
% TRIPOD TOP PLATE COORDINATES
```

```
C11=(-1*dC);                % C1X
C12=0;                  % C1Y
C13=0;                  % C1Z
C21=(dC/2);             %C2X
C22=(dC*((sqrt(3))/2));    %C2Y
C23=0;                  % C2Z
C31=(dC/2);                % C3X
C32=(-1*dC*((sqrt(3))/2));  % C3Y
C33=0;                  % C3Z

% TRIPOD BOTTOM PLATE COORDINATES (BASE INITIAL)
B11=(-1*dB);                % B1X
B12=0;                  % B1Y
B13=0;                  % B1Z
B21=(dB/2);             % B2X
B22=(dB*((sqrt(3))/2));     % B2Y
B23=0;                  % B2Z
B31=(dB/2);                 % B3X
B32=(-1*dB*((sqrt(3))/2));     % B3Y
B33=0;                  % B3Z

% FIND LINK LENGTH OF CURRENT POSE
Q6001=((L1/Q1)+Lmin); %Lenght of link 1
Q6002=((L2/Q2)+Lmin); %Lenght of link 2
Q6003=((L3/Q3)+Lmin); %Lenght of link 3
Q6006=(L6/Q6);

% INITIAL GUESSES
Q6020=KinPosAxisB;
Q6030=KinPosAxisA;
Q6010=(L6/Q6);
Q6090=(C8);

% SET CYCLE COUNTER TO ZERO
Q6200=0;
% OFFSET SUMMATION FOR XYZ AXES OF END EFFECTOR

O7=(O1+O4); % SUMMATION OF END EFFECTOR X OFFSETS
O8=(O2+O5); % SUMMATION OF END EFFECTOR Y OFFSETS
O9=(O3+O6); % SUMMATION OF END EFFECTOR Z OFFSETS
```

```
% ITERATION LOOP
while Q6200 < Q6201

%FIND DRIVEN INPUTS  FROM KNOWN INPUTS
Q1151=(C31+C21);            %C3X + C2X
Q1152=(C32+C22);            %C3Y + C2Y
Q1153=(C31−C21);            %C3X − C2X
Q1154=(C32−C22);            %C3Y − C2Y
Q1155=(cosd(Q6020));
Q1156=(cosd(Q6030));
Q1157=(sind(Q6020));
Q1158=(sind(Q6030));
Q1159=(((−1*Q1157*Q1158*Q1154)+((−1/(sqrt(3)))*Q1156*Q1152)+(−1*Q1155*Q1153)+((2/(s
(((−2/(sqrt(3)))*Q1156*C11)+((1/(sqrt(3)))*Q1156*Q1151)+(Q1157*Q1158*Q1153)+(−1*Q11
Q1191=(atand(Q1159));

% R_BC = R(BETA)(GAMMA)(ALPHAd) ROTATION MATRIX
Q1161=((((cosd(Q6020))*(cosd(Q1191)))+
(((sind(Q6020))*(sind(Q6030))*(sind(Q1191))))));
Q1162=(((−1*(cosd(Q6020))*(sind(Q1191)))+
(((sind(Q6020))*(sind(Q6030))*(cosd(Q1191))))));
Q1163=((sind(Q6020))*(cosd(Q6030)));
Q1171=((cosd(Q6030))*(sind(Q1191))) ;
Q1172=((cosd(Q6030))*(cosd(Q1191))) ;
Q1173=(−1*(sind(Q6030))) ;
Q1181=(((−1*(sind(Q6020))*(cosd(Q1191)))+
(((cosd(Q6020))*(sind(Q6030))*(sind(Q1191))))));
Q1182=((((sind(Q6020))*(sind(Q1191)))+
(((cosd(Q6020))*(sind(Q6030))*(cosd(Q1191))))));
Q1183=((cosd(Q6020))*(cosd(Q6030)));

% DRIVEN X AND Y
Q1198=((−1*Q1171*C11)+(−1*Q1172*C12)+(−1*Q1173*C13)) ; %Y
Q1197=(((1/(sqrt(3)))*((Q1198)+(Q1171*C21)+(Q1172*C22)+(Q1173*C23)))−((Q1161*C21)+(


Q6011=(Q6006+Q1191−Q6010) ;
Q6010=Q6010+Q6011;
```

```
% R_BC = R(BETA)(GAMMA)(ALPHA) ROTATION MATRIX

Q2311=((((cosd(Q6020))*(cosd(Q6010)))+
(((sind(Q6020))*(sind(Q6030))*(sind(Q6010))))));
Q2312=(((-1*(cosd(Q6020))*(sind(Q6010)))+
(((sind(Q6020))*(sind(Q6030))*(cosd(Q6010))))));
Q2313=((sind(Q6020))*(cosd(Q6030))) ;
Q2321=((cosd(Q6030))*(sind(Q6010))) ;
Q2322=((cosd(Q6030))*(cosd(Q6010))) ;
Q2323=(-1*(sind(Q6030))) ;
Q2331=(((-1*(sind(Q6020))*(cosd(Q6010)))+
(((cosd(Q6020))*(sind(Q6030))*(sind(Q6010))))));
Q2332=((((sind(Q6020))*(sind(Q6010)))+
(((cosd(Q6020))*(sind(Q6030))*(cosd(Q6010))))));
Q2333=((cosd(Q6020))*(cosd(Q6030))) ;

% CORRECTION FACTORS FOR R

Q2401=((O7)-((O7*Q2311)+(O8*Q2312)+(O9*Q2313))) ;
Q2402=((O8)-((O7*Q2321)+(O8*Q2322)+(O9*Q2323))) ;
Q2403=((O9)-((O7*Q2331)+(O8*Q2332)+(O9*Q2333))) ;

% LINK LENGTH SUB CALCULATIONS (CORRECTION ALPHA ONLY)
% EQUATION F PRELIMINARY
Q2511=((Q1197)+(Q1161*C11)+(Q1162*C12)+(Q1163*C13)-(B11)) ;
Q2512=((Q1198)+(Q1171*C11)+(Q1172*C12)+(Q1173*C13)-(B12)) ;
Q2513=((Q6090)+(Zmin)+(Q1181*C11)+(Q1182*C12)+(Q1183*C13)-(B13)+(Q2403));
Q2521=((Q1197)+(Q1161*C21)+(Q1162*C22)+(Q1163*C23)-(B21)) ;
Q2522=((Q1198)+(Q1171*C21)+(Q1172*C22)+(Q1173*C23)-(B22)) ;
Q2523=((Q6090)+(Zmin)+(Q1181*C21)+(Q1182*C22)+(Q1183*C23)-(B23)+(Q2403));
Q2531=((Q1197)+(Q1161*C31)+(Q1162*C32)+(Q1163*C33)-(B31)) ;
Q2532=((Q1198)+(Q1171*C31)+(Q1172*C32)+(Q1173*C33)-(B32));
Q2533=((Q6090)+(Zmin)+(Q1181*C31)+(Q1182*C32)+(Q1183*C33)-(B33)+(Q2403));

% ITERATION COUNTER
Q6200=Q6200+1 ;

% LINK LENGTH CALCULATIONS
```

```
Q6041=(sqrt((Q2511*Q2511)+(Q2512*Q2512)+(Q2513*Q2513))) ;
Q6042=(sqrt((Q2521*Q2521)+(Q2522*Q2522)+(Q2523*Q2523))) ;
Q6043=(sqrt((Q2531*Q2531)+(Q2532*Q2532)+(Q2533*Q2533))) ;

% CALCULATE DIFFERENCE IN ACTUAL AND PREDICTED LINK LENGTHS


Q6021=(Q6001-Q6041)/Q6023 ; % BETA GUESS
Q6031=(Q6002-Q6042)/Q6033 ; % GAMMA GUESS
Q6091=((Q6001+Q6002+Q6003)-(Q6041+Q6042+Q6043))/3/Q6093; % Z GUESS

% ADJUST GUESS ANGLE BY Q60X1
% EQUATION N
Q6020=Q6020+Q6021 ;
Q6030=Q6030+Q6031 ;
Q6090=Q6090+Q6091 ;

% UPDATE GUESS - Q1, Q2, Q3
% EQUATION O
C0 = Q6010 ; % ALPHA POSITION
C1 = Q6020 ; % BETA POSITION
C2 = Q6030 ; % GAMMA POSITION

% CALCULATE X, Y, Z
% EQUATION O
C6=((L4/Q4)-Q2401+Q1197) ; % X AXIS POSITION
C7=((L5/Q5)-Q2402+Q1198) ; % Y AXIS POSITION
C8=Q6090 ; % Z AXIS POSITION

end
```

## A.2 Inverse Kinematics

### inversekinematicsmain.m

```
C0 = Alpha_des;                    %Alpha Position
```

```
C1 = Beta_des;                          %Beta Position
C2 = Gamma_des;                      %Gamma Position
C6 = X_des;                               %X-Axis Position
C7 = Y_des;                               %Y-Axis Position
C8 = Z_des;                               %Z-Axis Position

for i = 1:length(C1)
[L1(i),L2(i),L3(i),L4(i),L5(i),L6(i)] =
 invmodular(C0(i),C1(i),C2(i),C6(i),C7(i),C8(i));
end
```

**invmodular.m**

```
function [L1, L2, L3, L4, L5, L6] = invmodular(C0, C1, C2, C6, C7, C8)

% SCALE FACTORS FOR CONVERTING MOTOR UNITS TO MM
Q1=1; %FOR AXIS 1
Q2=1 ; %FOR AXIS 2
Q3=1 ; %FOR AXIS 3
Q4=1; %FOR AXIS 4
Q5=1 ; %FOR AXIS 5
Q6=1; %FOR AXIS 6

% MECHANICAL COORD VALUES
Zmax=277.409215;     %Maximum Z Axis Position
Zmin=218.630447;     %Minimum Z Axis Position
Lmax=280.35;         %Maximum Limb Length
Lmin=222.35;         %Minimum Limb Length
dB=153;          %Bottom Plate Diameter
dC=112.5;            %Top Plate Diameter


% DEFAULT END EFFECTOR OFFSETS
O1=0;
O2=0;
O3=0;
O4=0;
O5=0;
```

```
O6=61;


% TRIPOD TOP PLATE COORDINATES
C11=(−1*dC);                % C1X
C12=0;                  % C1Y
C13=0;                  % C1Z
C21=(dC/2);             %C2X
C22=(dC*((sqrt(3))/2));    %C2Y
C23=0;                  % C2Z
C31=(dC/2);                 % C3X
C32=(−1*dC*((sqrt(3))/2));   % C3Y
C33=0;                  % C3Z

% TRIPOD BOTTOM PLATE COORDINATES (BASE INITIAL)
B11=(−1*dB);                 % B1X
B12=0;                   % B1Y
B13=0;                   % B1Z
B21=(dB/2);              % B2X
B22=(dB*((sqrt(3))/2));     % B2Y
B23=0;                   % B2Z
B31=(dB/2);                  % B3X
B32=(−1*dB*((sqrt(3))/2));     % B3Y
B33=0;                   % B3Z

% OFFSET SUMMATION FOR XYZ AXES OF END EFFECTOR

O7=(O1+O4); % SUMMATION OF END EFFECTOR X OFFSETS
O8=(O2+O5); % SUMMATION OF END EFFECTOR Y OFFSETS
O9=(O3+O6); % SUMMATION OF END EFFECTOR Z OFFSETS

%% FIND DRIVEN INPUTS (ALPHAd, Xd, Yd) FROM KNOWN INPUTS
Q1051=(C31+C21);         %%C3X + C2X
Q1052=(C32+C22);         %%C3Y + C2Y
Q1053=(C31−C21);         %%C3X − C2X
Q1054=(C32−C22);         %%C3Y − C2Y
Q1055=(cosd(C1));
Q1056=(cosd(C2));
Q1057=(sind(C1));
Q1058=(sind(C2));
```

```
Q1059=(((−1*Q1057*Q1058*Q1054)+((−1/(sqrt(3)))*Q1056*Q1052)+(−1*Q1055*Q1053)+((2/(s
Q1091=(atand(Q1059));

% R_BC = R(BETA)(GAMMA)(ALPHAd) ROTATION MATRIX
Q1061=((((cosd(C1))*(cosd(Q1091)))+
(((sind(C1))*(sind(C2))*(sind(Q1091))))))    ;
Q1062=(((−1*(cosd(C1))*(sind(Q1091)))+
(((sind(C1))*(sind(C2))*(cosd(Q1091))))));
Q1063=((sind(C1))*(cosd(C2)));
Q1071=((cosd(C2))*(sind(Q1091)));
Q1072=((cosd(C2))*(cosd(Q1091)));
Q1073=(−1*(sind(C2)));
Q1081=(((−1*(sind(C1))*(cosd(Q1091)))+
(((cosd(C1))*(sind(C2))*(sind(Q1091))))));
Q1082=((((sind(C1))*(sind(Q1091)))+
(((cosd(C1))*(sind(C2))*(cosd(Q1091))))));
Q1083=((cosd(C1))*(cosd(C2)));

%% DRIVEN Xd AND Yd
Q1098=((−1*Q1071*C11)+(−1*Q1072*C12)+(−1*Q1073*C13));            %%Yd
Q1097=(((1/(sqrt(3)))*((Q1098)+(Q1071*C21)+(Q1072*C22)+(Q1073*C23)))
−((Q1061*C21)+(Q1062*C22)+(Q1063*C23)));
Q1096=(((−1/(sqrt(3)))*((Q1098)+(Q1071*C31)+(Q1072*C32)+(Q1073*C33)))
−((Q1061*C31)+(Q1062*C32)+(Q1063*C33)));

%% DRIVEN INPUTS ARE
%% Q1091
%% Q1097 Xd
%% Q1098 Yd

%% R = R(BETA)(GAMMA)(ALPHA)

Q1311=((((cosd(C1))*(cosd(C0)))+(((sind(C1))*(sind(C2))*(sind(C0))))));
Q1312=(((−1*(cosd(C1))*(sind(C0)))+(((sind(C1))*(sind(C2))*(cosd(C0))))));
Q1313=((sind(C1))*(cosd(C2)));
Q1321=((cosd(C2))*(sind(C0)));
Q1322=((cosd(C2))*(cosd(C0)));
Q1323=(−1*(sind(C2)));
Q1331=(((−1*(sind(C1))*(cosd(C0)))+(((cosd(C1))*(sind(C2))*(sind(C0))))));
Q1332=((((sind(C1))*(sind(C0)))+(((cosd(C1))*(sind(C2))*(cosd(C0))))));
```

```
Q1333=((cosd(C1))*(cosd(C2)));

%% CORRECTION FACTORS FOR R(ALPHA)

Q1401=((O7)-((O7*Q1311)+(O8*Q1312)+(O9*Q1313)));          %% ur
Q1402=((O8)-((O7*Q1321)+(O8*Q1322)+(O9*Q1323)));          %% vr
Q1403=((O9)-((O7*Q1331)+(O8*Q1332)+(O9*Q1333)));          %% wr

%% LINK LENGTH SUB CALCULATIONS

Q1511=((Q1097)+(Q1061*C11)+(Q1062*C12)+(Q1063*C13)-(B11));
Q1512=((Q1098)+(Q1071*C11)+(Q1072*C12)+(Q1073*C13)-(B12));
Q1513=((C8)+(Zmin)+(Q1081*C11)+(Q1082*C12)+(Q1083*C13)-(B13)+(Q1403));
Q1521=((Q1097)+(Q1061*C21)+(Q1062*C22)+(Q1063*C23)-(B21));
Q1522=((Q1098)+(Q1071*C21)+(Q1072*C22)+(Q1073*C23)-(B22));
Q1523=((C8)+(Zmin)+(Q1081*C21)+(Q1082*C22)+(Q1083*C23)-(B23)+(Q1403));
Q1531=((Q1097)+(Q1061*C31)+(Q1062*C32)+(Q1063*C33)-(B31))    ;
Q1532=((Q1098)+(Q1071*C31)+(Q1072*C32)+(Q1073*C33)-(B32))    ;
Q1533=((C8)+(Zmin)+(Q1081*C31)+(Q1082*C32)+(Q1083*C33)-(B33)+(Q1403));

%% LINK LENGTH CALCULATIONS

Q1601=(sqrt((Q1511*Q1511)+(Q1512*Q1512)+(Q1513*Q1513)));
Q1602=(sqrt((Q1521*Q1521)+(Q1522*Q1522)+(Q1523*Q1523)));
Q1603=(sqrt((Q1531*Q1531)+(Q1532*Q1532)+(Q1533*Q1533)));

%% MOTOR CALCULATIONS (CORRECTION A,B,G)

    L1=((Q1601-Lmin)*Q1);            %% Limb 1 Position
    L2=((Q1602-Lmin)*Q2);            %% Limb 1 Position
    L3=((Q1603-Lmin)*Q3);            %% Limb 1 Position
    L4=((C6+Q1401-Q1097)*Q4);        %% X Position
    L5=((C7+Q1402-Q1098)*Q5);        %% Y Position
    L6=((C0-Q1091)*Q6);          %% Gamma Position
end
```